nature communications

Article

https://doi.org/10.1038/s41467-025-67246-x

Decreased scleral *Wnt5a*^{hi} fibroblasts exacerbate myopia progression by disrupting extracellular matrix homeostasis in mice

Received: 28 April 2025

Accepted: 25 November 2025

Published online: 16 December 2025

Check for updates

He Zhu[1,5], Wei Chen[2,5], Xuemei Ling[1,3,5], Shiming Jiao[1,3], Le Yu[1], Huihui Liu[1], Mengyi Ding[1], Fan Zhang[2], Yixin Zhou[1], Yulu Pan[1], Zhonglou Zhou[1,3], Jia Qu[1,3], Fei Zhao[1,3] ✉, Fuxin Zhao[1,3] ✉ & Xiangtian Zhou[1,3,4] ✉

Myopia is a common refractive error with high prevalence; its pathogenesis is poorly understood. Scleral single-cell RNA sequencing is used to determine whether there is an association between phenotypic heterogeneity of scleral fibroblasts and form-deprivation myopia in male mice. The number of unique *Wnt5a*-positive scleral fibroblasts is markedly lower in the form-deprived eyes, specifically in the temporal inner peripapillary sclera. Inhibition of *Wnt5a* expression by injection of sh*Wnt5a*-AAV within Tenon's capsule causes increased myopia progression, while decreasing COL1A1 protein content and collagen fibril diameter. Integrating scleral bulk RNA-seq data from sh*Wnt5a*-AAV injected male mice with data from scleral single-cell RNA sequencing in form-deprivation myopia mice, implicates the *Sparc* gene as a key downstream target of the Wnt5a signalling pathway. Tenon's capsule injection of sh*Sparc*-AAV induces myopia, decreases scleral COL1A1 content, and reduces collagen fibril diameter. These results demonstrate that scleral-specific fibroblasts manifesting high *Wnt5a* expression (*Wnt5a*^{hi} fibroblast) modulate homeostasis of the extracellular matrix, thus promoting myopia progression.

Myopia (also called near- or short-sightedness) is a highly prevalent refractive error. Its prevalence is predicted to rise to 49.8% across the globe by 2050, with high myopia (refractive error worse than −6.00 dioptres (D)) expected to reach 9.8%[1]. It is a major concern in East Asia, where more than 90% of senior high school and university students are myopic, thus reaching epidemic proportions[2,3]. High myopia usually includes complications such as choroidal neovascularisation, macular degeneration, retinal detachment, glaucoma, etc., which can result in irreversible vision loss and even blindness[4,5]. Despite its importance, however, its pathogenesis is poorly understood, and the existing therapeutic procedures are inadequate to control myopia.

Myopia is characterised mainly by excessive axial elongation and posterior scleral thinning; these aberrant effects are derived from abnormal visual stimulation transduced through the retina-choroid-

[1]State Key Laboratory of Eye Health, Oujiang Laboratory (Zhejiang Lab for Regenerative Medicine, Vision and Brain Health), Eye Hospital, Wenzhou Medical University, Wenzhou, China. [2]Key Laboratory of Biomechanics and Mechanobiology (Ministry of Education), Key Laboratory of Innovation and Transformation of Advanced Medical Devices (Ministry of Industry and Information Technology), National Medical Innovation Platform for Industry-Education Integration in Advanced Medical Devices (Interdiscipline of Medicine and Engineering), School of Engineering Medicine, Beihang University, Beijing, China. [3]Research Unit of Myopia Basic Research and Clinical Prevention and Control, Chinese Academy of Medical Sciences (2019RU025), Wenzhou, Zhejiang, China. [4]Present address: Department of Ophthalmology, State Key Laboratory of Eye Health, Ninth People's Hospital, Shanghai Jiao Tong University School of Medicine, Shanghai, China. [5]These authors contributed equally: He Zhu, Wei Chen, Xuemei Ling. ✉e-mail: zhaofei@eye.ac.cn; zhaofuxing12@163.com; zhouxt@shsmu.edu.cn

sclera signal cascade[6,7]. This condition is characterised by declines in scleral collagen synthesis and content in the posterior pole[7,8]. In the physiological state, the sclera of the posterior pole is relatively thicker than that in other regions, and it becomes thinner during myopia development. Collagen is, in general, a major component of the extracellular matrix (ECM), which is secreted by fibroblasts[9,10]. Scleral fibroblasts, as a major cell type in the sclera, maintain ECM homoeostasis and the scleral scaffold by secreting some essential ECM constituents, such as MMP2 and TIMP. Scleral fibroblasts also secrete certain cytokines that regulate functions of other scleral cells, maintain the local scleral microenvironment, and participate in the regulation of ECM homoeostasis[11–13]. While several biochemical signalling pathways, such as those involving TGF-β and HIF-1α, have been implicated in mediating scleral ECM, the precise mechanisms by which these signalling cascades exert their effects remain incompletely elucidated.

Studies have shown that fibroblasts exhibit high tissue-specific heterogeneity. Specific fibroblast subpopulations play important roles in maintaining ECM homoeostasis in different tissues. For example, damage-responsive fibroblasts, *En1*$^{+}$ fibroblasts, and *Hrc*^{hi} fibroblasts are characteristic of specific fibrotic lung diseases[14,15], myocardial fibrosis[16], tumour microenvironment[17], and skin wound healing[18]. The cellular heterogeneity and spatial distribution of fibroblasts may be involved in regulating the microenvironment and ECM homoeostasis in specific regions, thereby influencing tissue morphology and biological function. It has been shown previously that the myopic sclera is characterised by increased transdifferentiation of fibroblasts to myofibroblasts[19]. Nevertheless, whether specific fibroblast subpopulations are involved in myopia progression has yet to be clarified.

To achieve this goal, we mapped scleral gene expression patterns at single-cell resolution in form deprivation myopia (FDM) in mice. This undertaking revealed heterogeneity of scleral fibroblasts and identified a specific fibroblast subpopulation involved in myopia development and progression. This unique fibroblast subpopulation (*Wnt5a*$^{+}$) was decreased, and the non-canonical Wnt (ncWnt) signalling pathway was inhibited in form deprived (FD) eyes, indicating that this *Wnt5a*$^{+}$ fibroblast subpopulation might be involved in the development of myopia. In parallel, we confirmed that *Wnt5a*$^{+}$ fibroblasts were distributed mainly in the posterior pole of the sclera, and that the number of *Wnt5a*$^{+}$ fibroblasts declined during myopia progression. Furthermore, inhibition (by shRNA) and enhancement (by overexpression) of expression of *Wnt5a* and its downstream *Sparc*-gene-linked ECM modulation, by AAV sub-Tenon's capsule injection, directly affected refractive development as well as scleral collagen I synthesis and collagen ultrastructure. These results demonstrated that unique *Wnt5a*$^{+}$ fibroblasts highly expressing *Wnt5a* (named *Wnt5a*^{hi} fibroblast) in the posterior pole of the sclera, signalling via a Wnt5a pathway, promote myopia development by modulating scleral ECM homoeostasis.

Results

Single-cell expression profile characterisation uncovers variable scleral cell subtypes

Form deprivation myopia in 3-week-old C57BL/6 J mice was induced for 24 h or 48 h (from 9 a.m. 1 day, to 9 a.m. 1 or 2 days later). Sclerae were dissociated, and single cells were obtained. A 10× Genomics system was employed to perform scRNA-seq analysis (Fig. 1a) in four groups of scleral cells (FD treat-24 h, FD fellow-24 h, FD treat-48 h, and FD fellow-48 h; 'FD fellow' indicates non-FD contralateral eye). After applying quality control, we profiled a total of 39,884 cells from all samples, ranging in number from 7933 to 11,929. Unsupervised clustering revealed a total of 20 distinct cell populations (Fig. 1b). They were further separated into 10 cell types according to their expression profile similarities and the presence of diagnostic cell markers (Fig. 1b, c). The major cell types in the sclera are fibroblasts, vascular endothelial cells, and macrophages; muscle cells, keratocytes, neurons, and retinal pigment epithelium cells coming from the ciliary body, cornea, and pigment epithelium layer, respectively, might add contamination by non-scleral tissues. Fibroblasts were further analysed and re-clustered with increased resolution, revealing 16 subpopulations (Fig. 1d). We defined these 16 subtypes of scleral fibroblasts according to their specific markers or expression profiles (Fig. 1e, Supplementary Data 1). By combining scleral fibroblasts with other types of fibroblasts isolated from multiple mouse tissues, we observed that the majority of scleral fibroblasts formed a sclera-specific subtype, which is consistent with what is known about tissue-specificity[18,20] (Supplementary Fig. S1a). Besides, two universal fibroblast subtypes widely expressed in connective tissues (*Pi16*$^{+}$ and *Col15a1*$^{+}$) were also found in the sclera. The *Pi16*$^{+}$ subtype, which is stem-cell-like with high expression of *Pi16* and *Ly6a*, was designated cluster 14 in our scleral scRNA-seq catalogue. Cluster 7 of the scleral fibroblasts, which showed expression patterns similar to those of the *Col15a1*$^{+}$ subtype, but without significantly higher expression of *Col15a1* and *Penk*, was designated *Col15a1*-like in our analysis (Supplementary Fig. S1b).

Wnt5a^{+} fibroblast and ncWnt signalling decline significantly in the FD sclera

The changes in scleral cell composition during myopia development were examined further at each sampling time. Across all subtypes, we found that the proportion of cluster 11 (*Wnt5a*$^{+}$ fibroblast) showed a significant decrease after 24 h and 48 h of FD treatment ($P_{24h} = 5.5 \times 10^{-22}$ and $P_{48h} = 2.2 \times 10^{-80}$, Fig. 2a). A greater reduction in the numbers of *Wnt5a*$^{+}$ fibroblasts was observed at FD-48 h (8.35–0.91%) than at FD-24 h (2.96–0.80%), showing a continuous decrease in proportion of this cell subtype during the early stage of myopia development. Analysis of ECM interactions showed that the *Wnt5a*$^{+}$ fibroblast was mainly involved in collagen signalling (Fig. 2b). We analysed the single-nucleus RNA-sequencing data from human sclera[21], and found that *WNT5A* mRNA was expressed and *WNT5A*$^{+}$ fibroblasts account for 2% of total fibroblasts (Supplementary Fig. S2), which is compatible with murine sclera in our study.

To understand how declines in *Wnt5a*$^{+}$ fibroblasts affected the scleral microenvironment, we created a cell-cell communication network and estimated their differences between the FD-treated eye's sclera and the FD-fellow eye's sclera. The overall relative interaction strength of the noncanonical Wnt (ncWnt) signalling pathway was in sixth place across all secreted ligand-receptor pathways (Fig. 2c). The *Wnt5a*$^{+}$ fibroblasts provide the major signal of ncWnt ligands, and the major signal receivers are *Comp*$^{+}$, *Fzd1*$^{+}$, and *Igfbp2*$^{+}$ fibroblasts (Fig. 2c). In the ncWnt signalling pathway, Wnt5a and Wnt11 are the major ligands that interact with Fzd1 and Fzd2 as the major receptors (Fig. 2d). The subtype-specific marker gene (*Wnt5a*) of *Wnt5a*$^{+}$ fibroblasts is expressed mainly in this subtype, as well as at low levels in the *Pgf*$^{+}$, *Pi16*$^{+}$, and *Tagln*$^{+}$ fibroblasts (Fig. 2e). *Wnt11* expression is very low in all fibroblast subtypes (Fig. 2f). The scRNA-seq data analysis showed that the scleral *Wnt5a* mRNA level in FD-48h treated eyes was significantly less than that in FD-48h fellow eyes (Fig. 2g). Also, ncWnt signalling was inhibited in the FD-treated eye's sclera in both FD-24h and FD-48h (Fig. 2h).

RNA FISH validation of the *Wnt5a*$^{+}$ cluster was declined and WNT5A decreased by immunofluorescence labelling in FDM mice

According to the marker genes identified for each fibroblast subtype (Supplementary Data 1), *Wnt5a* and Alpha-2-Macroglobulin (*A2m*, which is the most significant upregulated marker gene) were selected as the markers of *Wnt5a*$^{+}$ fibroblasts. Their mRNA levels were analysed using RNA FISH (RNAscope). Firstly, *Wnt5a*$^{+}$ fibroblasts were identified by fluorescence microscopy in the murine sclera (Supplementary Fig. S3). According to ocular anatomical position (Fig. 3a), the *Wnt5a*$^{+}$ fibroblasts were distributed mainly in the posterior sclera (iPPS, oPPS), but scarcely in the peripheral sclera, during normal

https://doi.org/10.1038/s41467-025-67246-x

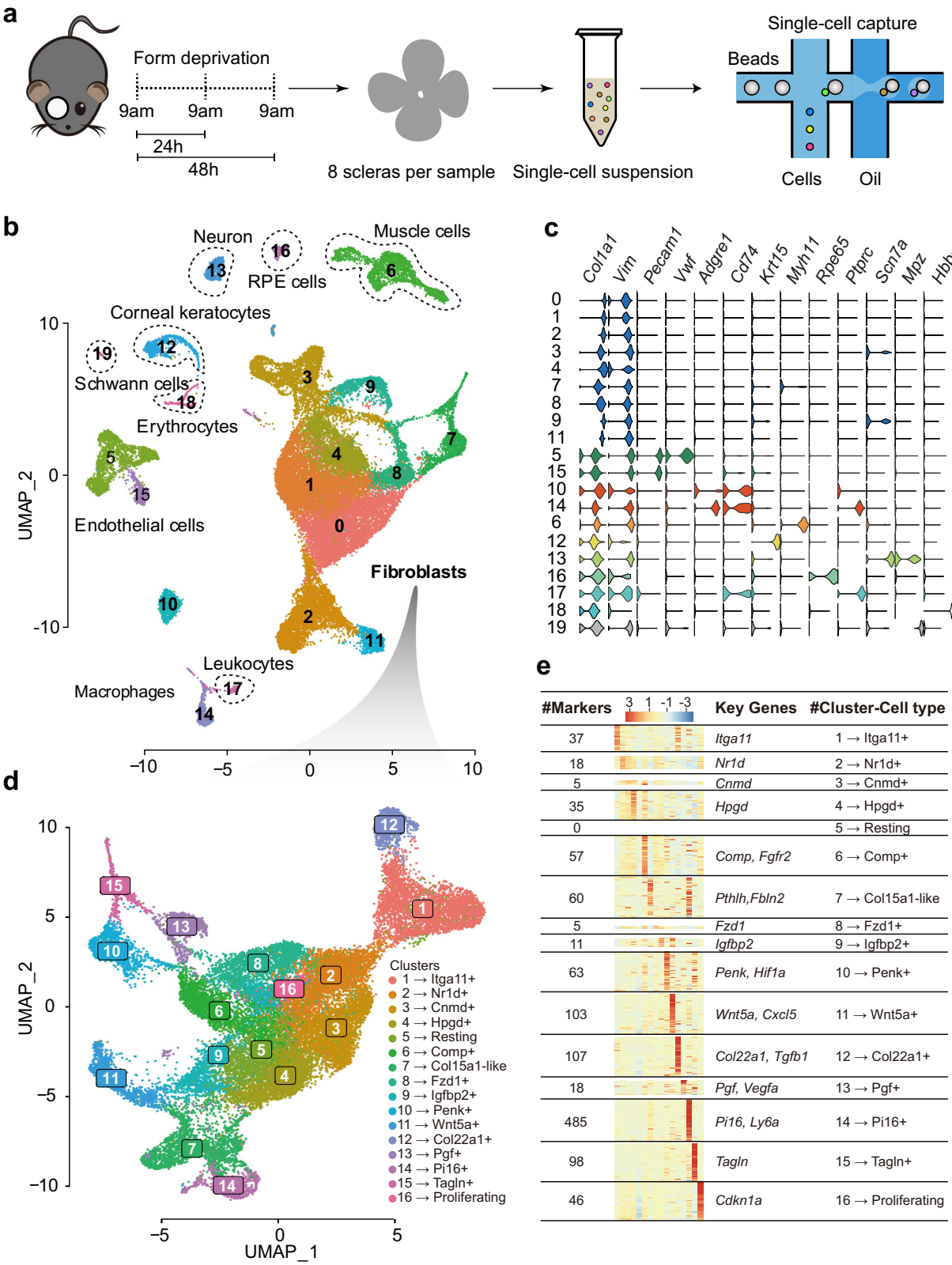

Fig. 1 | Single-cell transcriptome profiles of murine sclera from the form-deprived eyes and the fellow eyes. a The schematics of form deprivation treatment, scleral single cell dissociation, and single cell RNA sequencing in 10× Genomics. **b** The UMAP plot shows 20 cell clusters. These clusters are further separated into 10 major cell types. **c** Violin plots show the log-transformed expression level of canonical markers in each cluster. Different colours are used to distinguish between the 10 major cell types. **d** The UMAP plot shows 16 subtypes of scleral fibroblasts. **e** The heat map shows the relative average expression of the most strongly enriched genes and the key genes in each subtype of scleral fibroblasts. UMAP uniform manifold approximation and projection.

https://doi.org/10.1038/s41467-025-67246-x

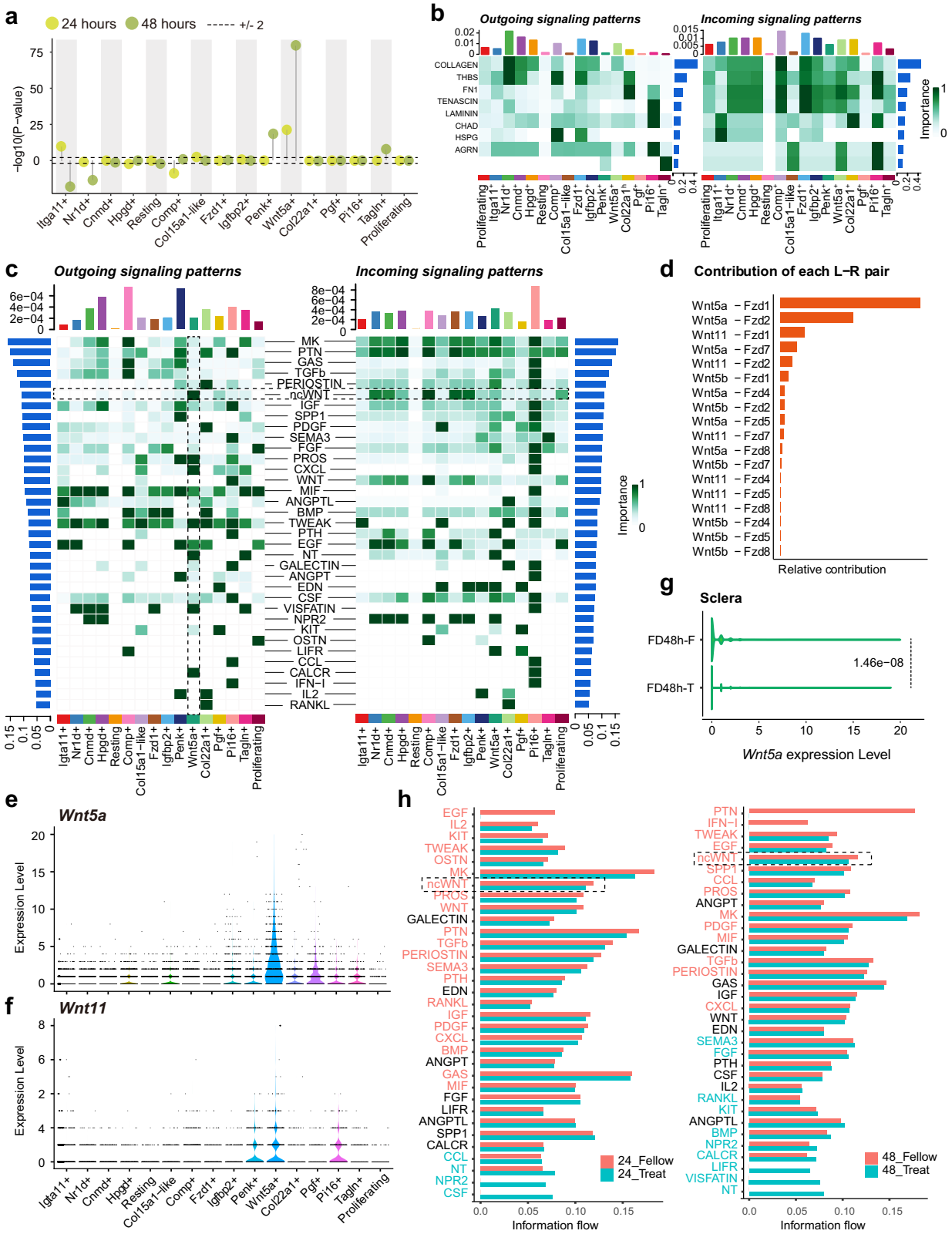

ocular development (Fig. 3b). In the temporal sclera of FD-treated eyes, the numbers and percentages of the *Wnt5a*$^+$ fibroblasts and *Wnt5a* puncta were significantly lower in the temporal iPPS of either FD-24h or FD-48h treated eyes than in that of the FD fellow eyes (Fig. 3c, d) or normal eyes (Fig. 3c, d). There were no statistically significant differences in the numbers and percentages of *Wnt5a*$^+$ fibroblasts and *Wnt5a* puncta in the oPPS and the peripheral sclera, among the FD-treated eyes, FD-fellow eyes, and normal control (NC) eyes, in either FD-24 h or FD-48 h, except for *Wnt5a* puncta in FD-24 h. In the nasal sclera, *Wnt5a* mRNA levels were unaltered in the iPPS and the peripheral sclera of FD-treated eyes, FD-fellow eyes, and NC eyes, in either FD-24 h or FD-48 h (Fig. 3d), except for the percentages of *Wnt5a*$^+$ fibroblasts in the iPPS and oPPS in FD-48 h. These results demonstrate that the *Wnt5a* mRNA expression pattern

Fig. 2 | Form-deprivation myopia induces dynamic changes and alterations of the cell-cell communication network in murine scleral fibroblasts. **a** Distribution of fibroblast subtypes expressed as a difference between FD-treated and FD-fellow sclera (two-sided chi-square test with Bonferroni correction for multiple testing). The X-axis indicates the subtypes corresponding to the uniform manifold approximation and projection plot. The Y-axis shows the log-transformed *P*-value obtained by the chi-square test between FD-treated and FD-fellow eyes' scleral fibroblast subtypes. Positive values indicate a decrease, whereas negative values indicate an increase in the FD-treated eyes when compared with the FD-fellow eyes. **b** Heat map of the ECM outgoing (left) and incoming (right) of cell-cell interaction in all fibroblast subtypes. **c** Heat map of the outgoing (left) and incoming (right) cell-cell interaction signals of all fibroblast subtypes. The row indicates the relative strength of each interaction pathway. The column indicates the total interaction strength of each fibroblast subtype. **d** Ligand-receptor pairs of the ncWNT signalling pathway of all fibroblast subtypes. The relative contribution of each ligand-receptor pair of the ncWNT signalling pathway among all scleral fibroblast subtypes. **e** Expression profile of *Wnt5a* of ncWNT signalling in each subtype of fibroblast. **f** Expression profile of *Wnt11* of ncWNT signalling in each fibroblast subtype. **g** *Wnt5a* mRNA level in FD-48h treated eyes and FD-48h fellow eyes (two-sided Wilcoxon signed-rank test). **h** Information flow of each cell–cell interaction pathway in FD treatment for 24 h or 48 h. FD form deprivation. Data are expressed as mean ± SEM.

declined as a function of spatiotemporal specificity in the sclera. Thus, this unique scleral *Wnt5a*$^+$ fibroblast-specific distribution pattern is correlated with myopia progression, suggesting the possibility of a causal relationship.

The *Wnt5a* mRNA level in the whole sclera, as bulk-detected by RT-qPCR, was downregulated in FDM mice after treatment for 2 weeks, but not after only 48 h (Fig. 3e). Using immunofluorescence to label the protein in scleral tissue sections (Fig. 3f), we showed that the WNT5A level was significantly higher in the iPPS than in the peripheral sclera in normal control mice (Fig. 3g). In FD-treated eyes, the WNT5A protein level in the temporal sclera was significantly less than that in the temporal iPPS in either FD-48 h or FD-2W treated eyes than in FD fellow eyes (Fig. 3h, i) or in the NC eyes (Fig. 3h, i). In the nasal sclera, WNT5A protein levels were unaltered in the iPPS, oPPS, or peripheral sclera among FD-treated eyes, FD-fellow eyes, and NC eyes in either FD-48 h or FD-2W (Fig. 3i) except for the iPPS in FD-48 h. The scleral WNT5A protein level decreased in FD-2W, but not in FD-48 h mice (Fig. 3j, k).

sh*Wnt5a*-AAV injection in mice induces myopia development, and si*Wnt5a* transfection in HSFs inhibits *Col1a1* expression

To shed light on whether *Wnt5a*$^+$ fibroblasts can induce myopia development in vivo, sh*Wnt5a* knockdown was used to model the inhibition of *Wnt5a*$^+$ fibroblast function. sh*Wnt5a*-AAV was delivered by a single sub-Tenon's capsule injection in 3-week-old C57BL/6 J mice, followed by refraction and ocular biometrics measurements at different intervals (Fig. 4a). Two weeks after sh*Wnt5a*-AAV injection, the whole sclera was infected by sh*Wnt5a*-AAV (Fig. 4b), and the scleral *Wnt5a* mRNA and WNT5A protein levels were downregulated in the sh*Wnt5a*-AAV injected eyes even after 6 weeks (Fig. 4c–e), whereas no changes in *Wnt5a* mRNA level were observed in the retina, cornea, or lens (Supplementary Fig. s4). Six weeks after sh*Wnt5a*-AAV infection, the refraction of the sh*Wnt5a*-AAV injected group had shifted significantly towards myopia (about −4.33 D in 4 W, −5.04 D in 6 W), significantly more than in the shScramble-AAV injected control group (Fig. 4f, AAV-4W; AAV-6W). Ocular axial elongation accompanied myopia development (Fig. 4g, AAV-6W). The *Col1a1*, but not *Acta2*, mRNA levels declined significantly in sh*Wnt5a*-AAV injected eyes (Fig. 4h). Similarly, the protein levels of COL1A1, but not α-SMA, were significantly reduced in the sh*Wnt5a*-AAV injected eyes (Fig. 4i, j), but not in the shScramble-AAV injected eyes. Transmission electron microscopy showed that the scleral collagen fibril diameter was thinner in the sh*Wnt5a*-AAV injected eyes than in the shScramble-AAV injected eyes (Fig. 4k).

Furthermore, COL1A1, MMP2, α-SMA, p-CaMK2A, CaMK2A, and β-Catenin protein levels were measured in human scleral fibroblasts (HSFs) after treatment with si*WNT5A* or si*WNT5A* + recombinant WNT5A (rWNT5A). WNT5A protein level was significantly inhibited in HSFs transfected with *WNT5A*-siRNA for 72 h (Supplementary Fig. S5a, b) and was reversed to some degree by adding rWNT5A (Supplementary Fig. S5a, b). *WNT5A*-siRNA interference decreased the COL1A1 protein level (Fig. S5a, b). rWNT5A rescued the declines in COL1A1 protein content caused by *WNT5A*-siRNA (Supplementary Fig. S5a, b). *WNT5A*-siRNA transfection with or without rWNT5A treatment did not alter MMP2 or α-SMA protein levels in HSFs. *WNT5A*-siRNA interference did not affect the canonical Wnt signal molecule, β-Catenin, but inhibited the synthesis of the non-canonical Wnt signalling molecule, p-CaMK2A (Supplementary Fig. S5c, d). In the sh*Wnt5a*-AAV injected mice, p-CaMK2A and CaMK2A protein levels were decreased, but β-Catenin was not altered (Supplementary Fig. S5e, f). Overall, these findings imply that *WNT5A* inhibition can reduce the synthesis, but not the degradation of COL1A1 via the Wnt5a-CaMKII signalling pathway.

Overexpression of *Wnt5a* by scleral AAV injection inhibited FDM but did not affect normal refractive development in mice

In addition, we constructed a scleral-overexpression *Wnt5a*-AAV mouse model by injecting 3-week-old mice with *Wnt5a*-AAV. Six weeks after sub-Tenon's injection, both the scleral *Wnt5a* mRNA (Fig. 5a) and WNT5A protein expression levels significantly increased more in the *Wnt5a*-AAV injected eyes than in the Vector-AAV injected control eyes (Fig. 5b, c). Firstly, 1 week after *Wnt5a*-AAV sub-Tenon's injections in 3-week-old mice, FD was initiated, and then FDM developed for another 2 weeks (Fig. 5d). We observed that *Wnt5a* overexpression induced by sub-Tenon's AAV injection inhibited FDM development (Fig. 5e). The OE*Wnt5a*-AAV injection group showed a statistically significant reduction of axial length compared with the vector-AAV injection group (Fig. 5f), and OE*Wnt5a*-AAV injection partly rescued the decrease in COL1A1 protein level that was caused by FD (Fig. 5g, h). During normal refractive development in mice (Fig. 5i), the overexpression of *Wnt5a* did not affect normal refractive development and axial elongation 6 weeks after *Wnt5a*-AAV (OE*Wnt5a*-AAV) injection (Fig. 5j, k).

Scleral bulk RNA-seq analysis in sh*Wnt5a*-AAV injected mice reveals that *Sparc* is a key downstream target gene of the Wnt5a

After performing sequence alignment, assembly, data quality control, and filtering, the differentially expressed genes (DEGs) were analysed in both sh*Wnt5a*-AAV and shScramble-AAV injected mice. Gene ontology (GO) and Reactome functional enrichment analysis showed that the most significantly downregulated pathways were related to ECM organisation and collagen biosynthesis (Fig. 6a, b). The results are illustrated in the heatmap of DEGs of the ECM pathway (Fig. 6c). The top DEGs from the ECM pathway (*Sparc*, *Adamts2*, *Pcolce2*, *Pcolce*, *Bmp1*, *Itga2*) were downregulated in the sclera of sh*Wnt5a*-AAV injected mice (Fig. 6d), as validated using RT-qPCR. These results indicate that *Wnt5a* may be a master gene that can regulate the development of ECM molecular expression patterns. Furthermore, to find the relationship of *Wnt5a* with these DEGs, hdWGCNA were constructed in *Wnt5a*$^+$ fibroblasts using scRNA Seq data. Seven co-expression gene modules were obtained (Supplementary Fig. S6a–c). *Wnt5a* was assigned to a gene module with eigengene-based kME = 0.394 (Supplementary Data 2). The function of this module was enriched in ECM organisation and autophagy-related pathways (Fig. 6e, f). *Sparc* appeared as the top hub gene of module 1 (kME = 0.776, Fig. 6e, Supplementary Data 2). And module 1 was significantly downregulated in

https://doi.org/10.1038/s41467-025-67246-x

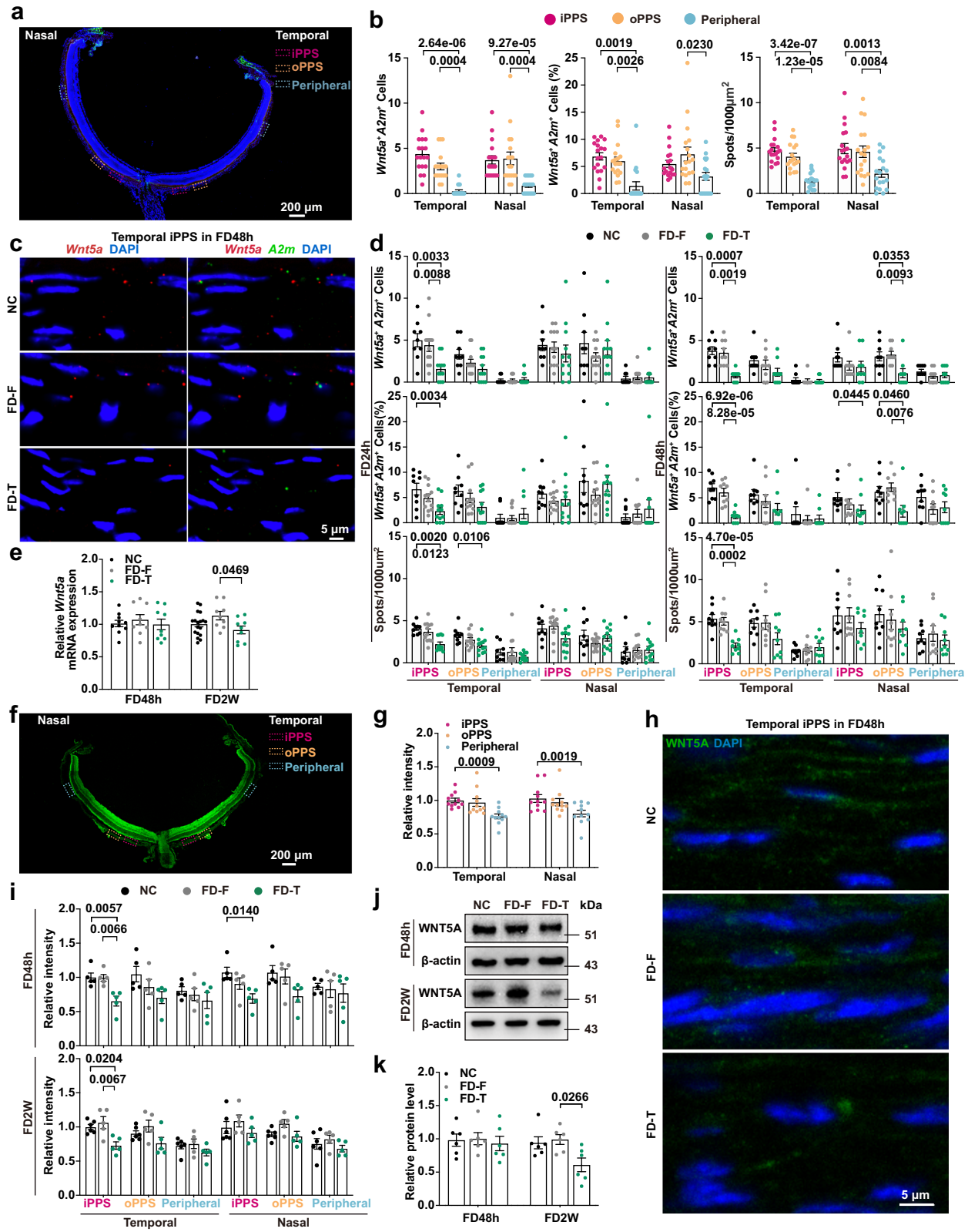

FD-treated sclera in comparison with FD-fellow sclera ($P = 9.5 \times 10^{-4}$, two-sided Wilcoxon signed-rank test, Supplementary Fig. S6c). These results indicated that *Sparc* is one of the key genes of the Wnt5a signalling pathway. We confirmed further that the scleral SPARC protein level was reduced more in the sh*Wnt5a*-AAV injected eyes than in the sh*Wnt5a*-AAV injected fellow eyes (Fig. 6g). Immunofluorescence labelling (Fig. 6h) showed that the SPARC protein level was significantly less in the temporal iPPS of FD-treated eyes than in that of non-FD fellow eyes (Fig. 6i) or the NC eyes (Fig. 6i). The SPARC protein level was significantly decreased in the temporal oPPS in FD-48 h treated eyes than in FD-48 fellow eyes (Fig. 6i). In the nasal sclera, SPARC protein levels were not altered in the iPPS, oPPS, or peripheral sclera in FD-treated eyes, FD-fellow eyes, and NC eyes after either FD-48 h or FD-2W (Fig. 6i).

Fig. 3 | Scleral *Wnt5a*$^+$ cluster alteration in FDM mice using RNAscope, and scleral WNT5A protein level change in FDM mice by immunofluorescence and western blot. a Locations of regionally differentiated sclera: iPPS, oPPS, and peripheral sclera. **b** Alteration of the number and percentage of *Wnt5a*$^+$*A2m*$^+$ cells and *Wnt5a*$^+$ puncta in the temporal and nasal iPPS, oPPS, and peripheral sclera in normal murine eyes at age 3 weeks. $n = 18$ micrographs; Friedman test with Dunn's post hoc test (two-sided) or RM-ANOVA with Bonferroni's post hoc test (two-sided). **c**, **d** The numbers and percentages of *Wnt5a*$^+$*A2m*$^+$ cells and *Wnt5a*$^+$ puncta in the temporal/nasal iPPS, oPPS, and peripheral sclera in NC eyes, FD-F eyes, and FD-T eyes. $n = 9$ micrographs for NC eyes; for FD eyes, n = 12 micrographs in FD-24h and n = 9 micrographs in FD-48h, one-way ANOVA with Bonferroni's post hoc test or Kruskal-Wallis non-parametric test with Dunn's post hoc test (two-sided). **e** The *Wnt5a* mRNA level in NC eyes, FD-F eyes, and FD-T eyes treated by FD-48 h or FD-2W. For NC eyes, n = 10 in FD-48 h and $n = 18$ in FD-2W; for FD-F eyes and FD-T eyes, $n = 9$; one-way ANOVA with Bonferroni's post hoc test. WNT5A protein immunofluorescence intensity (**f**) and distribution (**g**) in the temporal/nasal iPPS, oPPS, and peripheral sclera in normal murine eyes. $n = 11$, Friedman tests with Dunn's post hoc tests (two-sided). WNT5A protein immunofluorescent intensity (**h**) and change (**i**) in the temporal/nasal iPPS, oPPS, and peripheral sclera in NC eyes, FD-F eyes, and FD-T eyes. For NC eyes, n = 5 in FD-48 h and $n = 6$ in FD-2W; for FD-F eyes and FD-T eyes, $n = 5$, one-way ANOVA with Bonferroni's post hoc test or Kruskal–Wallis non-parametric test with Dunn's post hoc test (two-sided). Western blots (**j**) and densitometric quantification (**k**) of scleral WNT5A protein in FDM mice. $n = 6$, one-way ANOVA with Bonferroni's post hoc test (two-sided). red: *Wnt5a*; green: *A2m*; blue: 4', 6-diamidino-2-phenylindole (DAPI), iPPS the inner peripapillary sclera, oPPS the outer peripapillary sclera, peripheral the peripheral sclera. NC normal control eyes, FD-F untreated contralateral eyes of form deprivation mice, FD-T form-deprived eyes. Data are expressed as mean ± SEM.

sh*Sparc*-AAV sub-Tenon's injection downregulates *Col1a1* gene expression and induces myopia in mice

To clarify further whether Wnt5a-induced disruption of ECM homoeostasis promotes myopia progression via *Sparc* gene regulation, sh*Sparc*-AAV was injected via sub-Tenon's capsule in 3-week-old C57BL/6 J mice (Fig. 7a). Six weeks after sh*Sparc*-AAV injection, the scleral *Sparc* mRNA levels (Fig. 7b) and protein levels (Fig. 7c, d) were significantly less in sh*Sparc*-AAV injected eyes than in shScramble-AAV injected eyes or sh*Sparc*-AAV injected fellow eyes. These results showed that sh*Sparc*-AAV injection successfully inhibited scleral *Sparc* expression. And *Col1a1* expression level was downregulated (Fig. 7b–d). After 6 weeks of sh*Sparc*-AAV infection, the refraction of the sh*Sparc*-AAV injection group shifted markedly towards myopia (about −2.31 D in 4 W post-sh*Sparc*-AAV injection, −4.89 D in 6 W post-sh*Sparc*-AAV injection) compared with the shScramble-AAV injection group (Fig. 7e, AAV-6W). Ocular biometric measurements results showed a significant increase of axial length in the sh*Sparc*-AAV injection group than in the shScramble-AAV injection group (Fig. 7f, AAV-6W). Scleral transmission electron microscopy analysis showed that the scleral collagen fibril diameter was thinner in the sh*Sparc*-AAV injected eyes than in the shScramble-AAV injected eyes (Fig. 7g).

Furthermore, 72 h after si*SPARC* transfection of the HSFs, the COL1A1 protein level was significantly reduced (Supplementary Fig. S7a, b), but not the α-SMA protein. Immunofluorescence labelling also showed that this treatment diminished COL1A1 protein content in the HSFs (Supplementary Fig. S7c, d).

Inhibition of *Wnt5a*^{hi} fibroblast gene expression exacerbates myopia progression by downregulating the Wnt5a-CaMKII-ECM signalling pathway

The insight obtained from this study is sufficient for constructing a working model that summarises our findings. This is illustrated in Fig. 8, wherein abnormal visual stimulation traversing the retina-choroid-sclera cascade suppresses *Wnt5a*^{hi} fibroblast gene expression. This effect reduces WNT5A secretion, and in turn, inhibits the non-canonical Wnt signalling pathway (Wnt5a-Ca^{2+}- CaMKII). Subsequently, downregulation of CaMKII via an indirect pathway may result in expression of genes for ECM molecules, such as *Col1a1*, *Sparc*, *Pcolce*, *Pcelce2*, *Adamts2*, *Bmp1*, and *Igta2*. This response may disrupt ECM structural organisation, give rise to collagen I decline, and a reduction in the collagen fibril diameter, finally resulting in scleral ECM homeostasis imbalance and causing myopia progression. These results highlight a role for *Wnt5a*^{hi} fibroblast heterogeneity in modulating scleral ECM homeostasis and myopia development.

Discussion

Decrease of a unique scleral fibroblast subpopulation induces myopia through disruption of ECM homeostasis

Single-cell RNA sequencing (scRNA-seq) technology uncovers the composition of different cell types and functions within highly organised tissues/organs/organisms[22]. Using this technology, we defined 16 subtypes of fibroblasts in the murine sclera. Some universal subtypes (*Pi16*$^+$ and *Col15a1*$^+$) of fibroblasts are also found in the murine sclera and other tissues[23]. Nevertheless, the majority of formed scleral fibroblasts had origins similar to those observed in tendons and bones. This finding is consistent with the known characteristics of fibroblasts' tissue specificity[23]. These properties suggest that murine scleral fibroblasts are endowed with both pan- and tissue-specific characteristics.

We observed that the cell number of the *Wnt5a*$^+$ fibroblast subtype declined significantly over time in the sclera of FDM murine eyes. This gave rise to declines in WNT5A, resulting in a reduction of both scleral collagen content and progression of myopia. There is evidence to suggest that hypoxia regulates *Wnt5a* expression[24,25]. Scleral hypoxia promotes myopia development[19,26]. Therefore, we speculate here that myopiagenic visual stimuli suppress choroidal blood flow, which leads to scleral hypoxia, and that this, in turn, inhibits *Wnt5a* expression and both hinders the differentiation and reduces the number of *Wnt5a*$^+$ fibroblasts. On the other hand, some studies have shown that TGF-β can elevate *Wnt5a* expression[27,28]. Increased scleral TGF-β expression promoted myopia progression, whereas declines in TGF-β inhibited myopia and downregulated Wnt5a[29,30]. This effect led to an obstruction of *Wnt5a*$^+$ fibroblast differentiation and a decline in their cell number.

In the present study, the scleral bulk RNA-seq in sh*Wnt5a*-AAV injected mice showed that some ECM molecules involved in procollagen cleavage, assembly, and secretion (including Sparc, Pcolce, Pcelce2, Adamts2, Bmp1, and Igta2) were significantly downregulated in sh*Wnt5a*-AAV Tenon's capsule-injected eyes. The *Sparc* gene encodes a cysteine-rich acidic matrix-associated protein, as an anti-adhesive glycoprotein, which is involved in collagen synthesis and assembly, and fibrosis[31,32]. It has been reported that *Sparc* was downregulated in minus-lens-, but not plus-lens-treated tree shrew eyes[33–35]. In the present study, sub-Tenon's capsule injection of sh*Sparc*-AAV selectively knocked down scleral *Sparc* gene expression, downregulated the COL1A1 levels, and reduced the collagen fibril diameter in the sclera, leading to myopia. This suggests that Wnt5a can modulate *Sparc* gene expression, which in turn regulates collagen synthesis and secretion, consequently impacting ECM turnover. In addition, it was observed that the inhibition of *Wnt5a* gene expression directly downregulated the expression of scleral genes for collagen cleavage molecules, specifically the N peptidase *(Adamts2)* and C peptidase (*Bmp1*, *Pcolce*, *Pcolce2*). This led to the inhibition of cleavage of the N- and C-terminals of procollagen, consequently preventing procollagen from assembling into mature collagen fibres. Overall, these combined effects, such as suppression of scleral collagen synthesis and reduction in its content, disorganisation of fibrils and diminution of fibril diameter, and the decline in ECM stiffness, have the potential to exacerbate myopia development. This finding suggests that *Wnt5a* may be a master gene that regulates the composition and biomechanical

https://doi.org/10.1038/s41467-025-67246-x

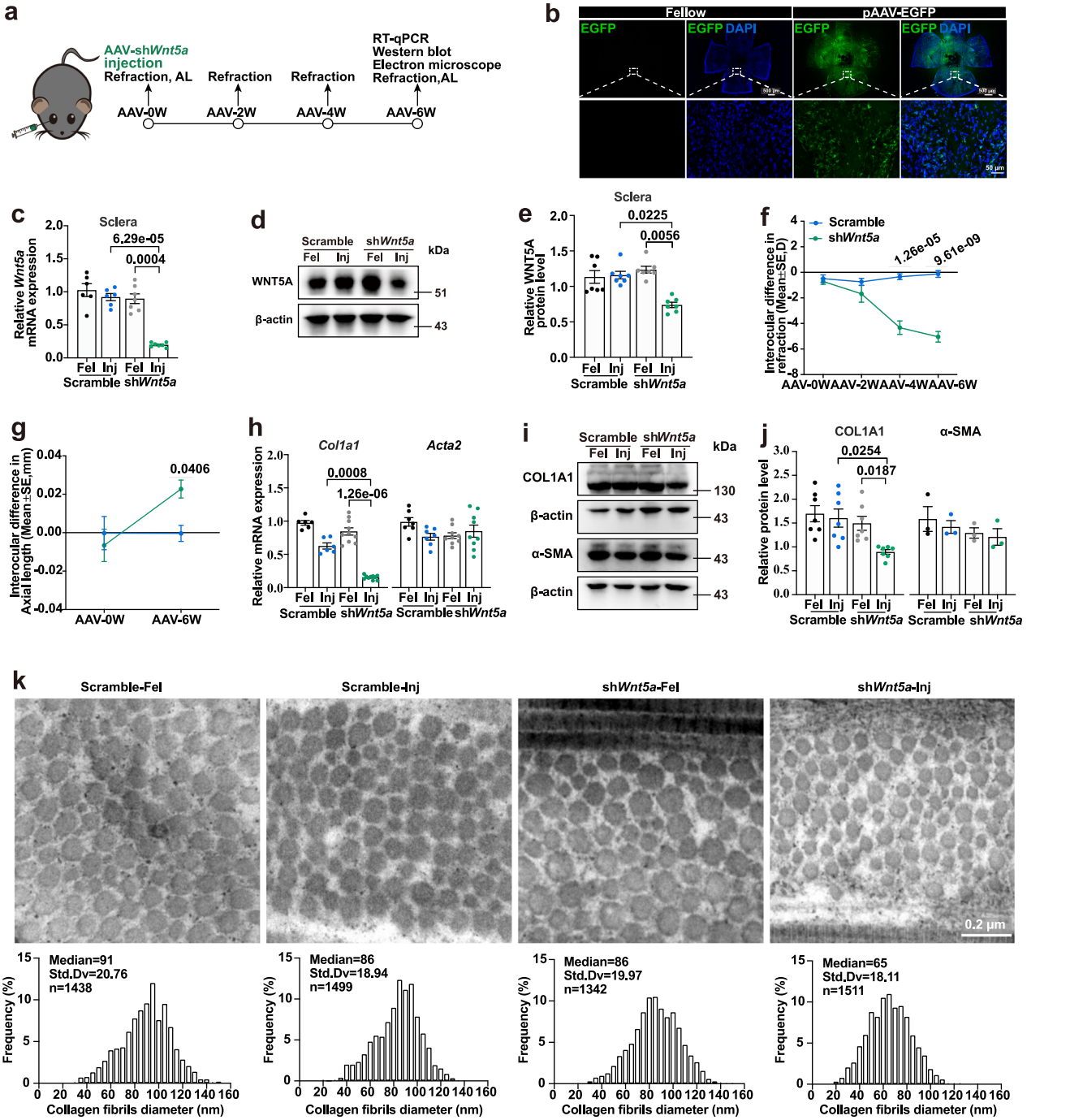

Fig. 4 | Construction of the *Wnt5a* knockdown model using sh*Wnt5a*-AAV sub-Tenon's injection in mice, the refractive development state and scleral collagen fibril structure of the sh*Wnt5a*-AAV injected mice. a sh*Wnt5a*-AAV injection and refraction and ocular biometrics measurements were carried out at different time points. **b** AAV infection in the whole murine sclera after sh*Wnt5a* sub-Tenon's injection. **c** The scleral *Wnt5a* mRNA level declined by sh*Wnt5a*-AAV injection. $n = 6$ for sh*Scramble*-AAV injected group and $n = 7$ for sh*Wnt5a*-AAV injected group, Brown-Forsythe and Welch ANOVA tests with Dunnett's T3 post hoc test (two-sided). **d**, **e** WNT5A protein levels were significantly downregulated by sh*Wnt5a*-AAV injection. $n = 7$ mice per group, Friedman test with Dunn's post hoc test (two-sided). **f** The refraction of sh*Wnt5a*-AAV injected eyes underwent a greater myopic shift than did the shScramble-AAV injected mice. $n = 15$ for the shScramble-AAV injected group and $n = 13$ for the sh*Wnt5a*-AAV injected group, two-way repeated measures ANOVA with Bonferroni's post hoc test. **g** Compared with shScramble-AAV infection, sh*Wnt5a*-AAV infection caused a significant increase in axial length. $n = 15$ for the shScramble-AAV injected group and $n = 13$ for the sh*Wnt5a*-AAV injected group, two-way repeated measures ANOVA with Bonferroni's post hoc test. *Col1a1* and *Acta2* mRNA (**h**, for *Col1a1*, $n = 6$ for shScramble-AAV injected group and $n = 10$ for sh*Wnt5a*-AAV injected group, Brown-Forsythe and Welch ANOVA tests with Dunnett's T3 post hoc test, two-sided; for *Acta2*, $n = 7$ for shScramble-AAV injected group and $n = 9$ for sh*Wnt5a*-AAV injected group, one-way ANOVA with Bonferroni's post hoc test, two-sided) and protein (**i**, **j**, $n = 7$ for COL1A1 and n = 3 for α-SMA, RM-ANOVA with Bonferroni's post hoc test (two-sided) for COL1A1 and Friedman test with Dunn's post hoc test (two-sided) for α-SMA) level in shScramble-AAV, sh*Wnt5a*-AAV injected mice. **k** scleral fibril ultrastructure and scleral fibril diameter of the fellow eyes and the treated eyes in shScramble-AAV injected mice and sh*Wnt5a*-AAV injected mice ($n = 3$ mice per group). Data are expressed as mean ± SEM.

https://doi.org/10.1038/s41467-025-67246-x

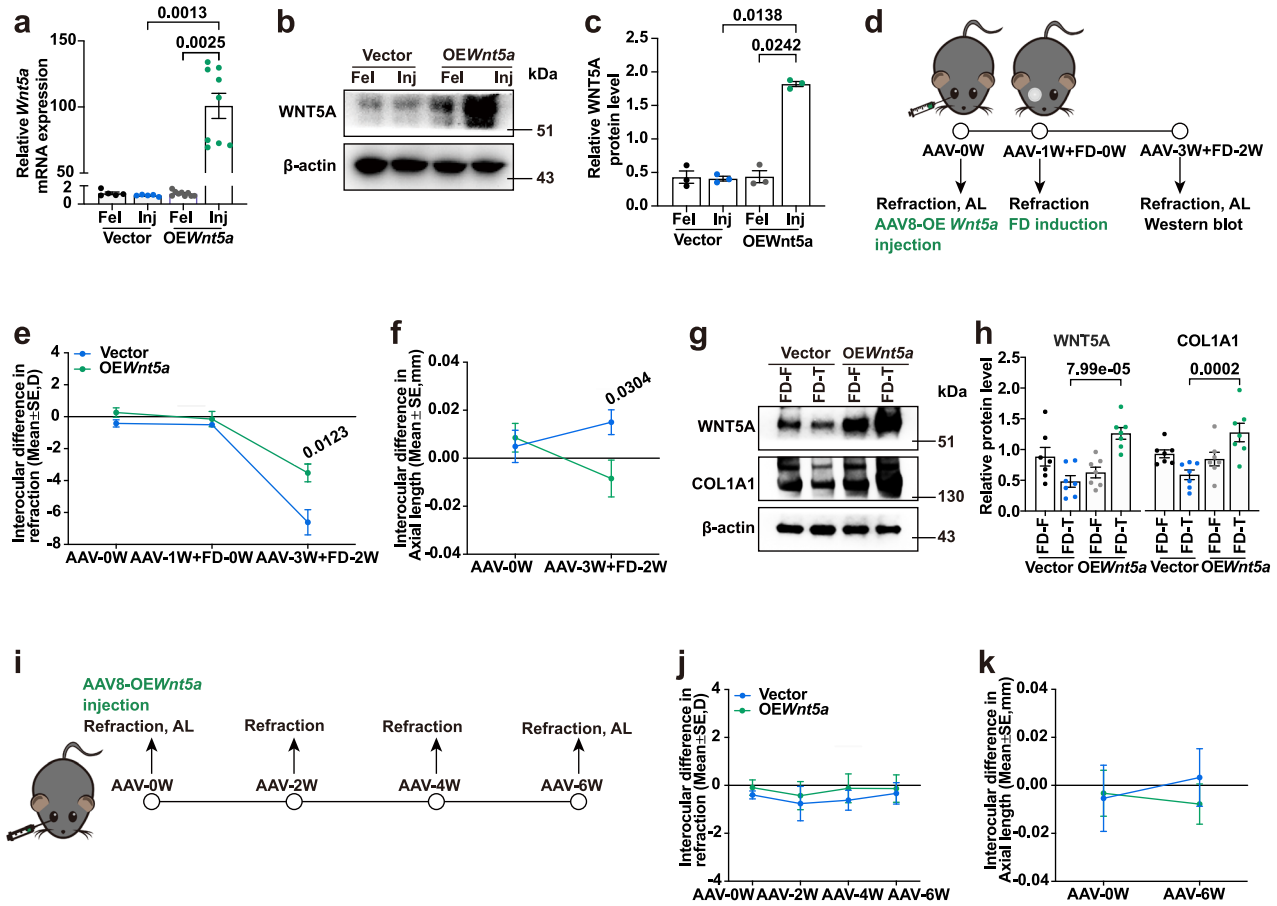

Fig. 5 | Changes in refraction and ocular biometrics in vector-AAV- and OE*Wnt5a*-AAV injected mice. Six weeks after sub-Tenon injection of OE*Wnt5a*-AAV, *Wnt5a* was overexpressed in the sclera at mRNA (**a**, $n = 5$ for vector -AAV injected group and $n = 9$ for OE*Wnt5a* -AAV injected group, Kruskal–Wallis non-parametric test with Dunn's post hoc test) and protein levels (**b**, **c**, $n = 3$, RM-ANOVA with Bonferroni's post hoc test, two-sided). **d** Schematic schedule of FD treatment and *Wnt5a* overexpression with AAV injection. In the FDM mouse model, OE*Wnt5a*-AAV injected + FDM mice developed less myopic shift than did the vector-AAV injected mice (**e**). In comparison with the vector-AAV injected eyes, OE*Wnt5a*-AAV injected + FD eyes exhibited a significant difference for axial length (**f**, $n = 13$ for vector-AAV injected group and $n = 16$ for OE*Wnt5a*-AAV injected group, two-way repeated measures ANOVA with Bonferroni's post hoc tests, two-sided, for refraction and for axial length). **g**, **h** *Wnt5a* overexpression can partially rescue the COL1A1 protein level, which is downregulated by FD. $n = 7$, ordinary two-way ANOVA with Bonferroni's post hoc test (two-sided). In mice undergoing normal refractive development (**i**), sub-Tenon's injection of OE*Wnt5a*-AAV did not affect refraction (**j**) or axial length (**k**). $n = 11$ for the vector-AAV injected group and $n = 15$ for the OE*Wnt5a*-AAV injected group, two-way repeated measures ANOVA with Bonferroni's post hoc test (two-sided). FD form deprivation; FDM form deprivation myopia. Data are expressed as mean ± SEM.

properties of scleral ECM; thus, Wnt5a may play a pivotal role in the maintenance of ECM homeostasis.

The alterations of posterior pole sclera that are consistent with the characteristics of myopia include lowering of collagen expression, thinning of collagen fibril diameter, and axial elongation[7,36]. Our findings demonstrate that *Wnt5a*$^+$ fibroblasts are associated with a posterior pole-specific decrease in myopia. The distribution and changes of *Wnt5a*$^+$ fibroblasts in the sclera closely mirror the pattern of pathological changes in myopia, providing compelling evidence that the *Wnt5a*$^+$ fibroblasts play a crucial role in the development of myopia.

WNT5A, as a ligand, is involved in the Wnt signalling pathway, and it has been reported that the Wnt signalling pathway is associated with myopia. The *WNT7B* gene (a canonical part of the Wnt signalling pathway) was identified as a myopic susceptibility gene in the human population using meta-GWAS analysis[37,38]; the *WNT7B* variant increases the corneal curvature, leading to myopia. In animal models of myopia (mice, guinea pigs and rats), the canonical Wnt pathway was also altered in the retina[39,40], sclera[41,42], and choroid[43]; but the upstream triggers and anatomical sources responsible for initiating these changes have not been identified.

In humans, *WNT5A* mRNA was expressed in the sclera, and *WNT5A*$^+$ fibroblasts accounted for 2% of total fibroblasts in human sclera by single-nucleus RNA-sequencing[21]. Genetically, there is not yet any direct evidence that *WNT5A* and *SPARC* are associated with human myopia, although large-scale genome-wide association studies have identified some genes (*NFATC3*, *RHOA*, and *TCF7L2*) involved in the ncWNT signalling pathway that are associated with myopia susceptibility[44]. Therefore, gene-set-based association analysis is needed in future studies to ensure the contribution of ncWNT signalling to genetic susceptibility to myopia in the whole pathway.

Altogether, using single-cell RNA sequencing and biochemical validation assays, we have revealed significant heterogeneity among scleral fibroblasts. Specifically, reduced secretion of WNT5A, due to the decline of *Wnt5a*$^+$ fibroblasts that typically express high levels of *Wnt5a*, accounts for the overall downregulation of scleral Wnt5a expression, resulting in an imbalance of scleral ECM homeostasis and thereby inducing myopia. These results identify the cellular origin of Wnt5a downregulation. Additionally, the findings suggest that Wnt5a may serve as a novel potential target for myopia intervention.

https://doi.org/10.1038/s41467-025-67246-x

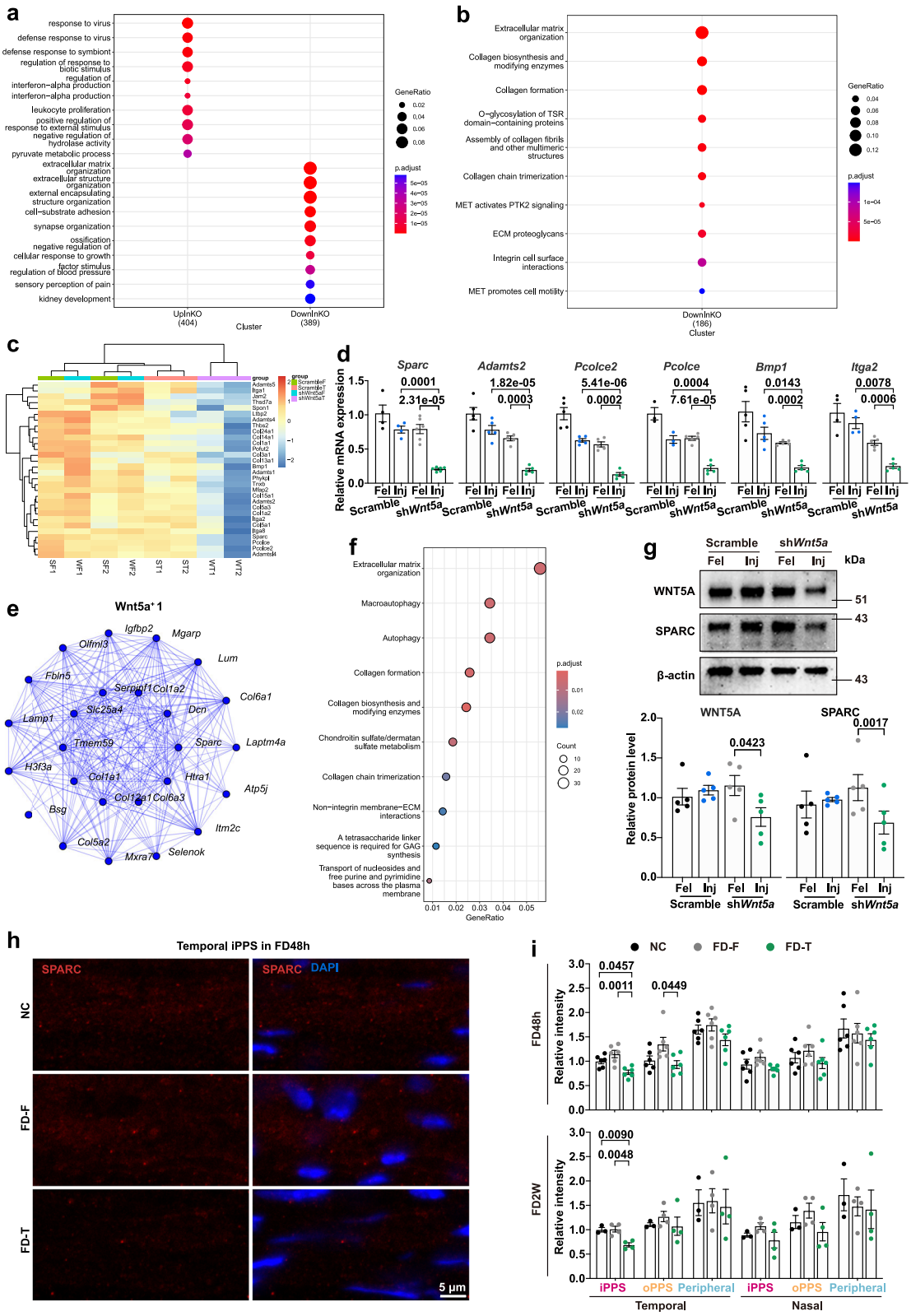

Spatio-specific *Wnt5a*$^{+}$ fibroblast localisation affects scleral physiological structures underlying myopia progression

Scleral thickness is asymmetric in normal development. The posterior sclera is relatively thicker than the equatorial and anterior regions[7,45]. Asymmetry is also characteristic of some organs and tissues, such as the heart and kidney. Its mechanism involves the Wnt5a/planar cell polarity (PCP) signalling cascade[46,47], and PCP signal activation depends on a concentration gradient of WNT5A. Wnt5a has been demonstrated to modulate polarity-associated gene expression via the Wnt5a/PCP signalling pathway, which then influences cell polarity and migration, and the development of organ asymmetry[48–50]. During the ocular developmental process, the sclera is initially composed of neural crest cells and mesenchymal cells of the optic cup, which gradually differentiate starting from the corneoscleral limbus to the

Fig. 6 | Bioinformatic analysis and validation of scleral bulk RNA-seq of sh*Wnt5a*-AAV sub-Tenon's injection. a, **b** Gene ontology (GO) and Reactome pathway analysis of differentially expressed genes (DEGs) from scleral bulk RNA-seq after sub-Tenon's injection of sh*Wnt5a*-AAV ($n = 2$ each group, one-sided hyper-geometric test with Benjamini-Hochberg correction for multiple testing). **c** DEGs heatmap of the ECM pathway from scleral bulk RNA-seq analysis. **d** Reverse Transcription quantitative Polymerase Chain Reaction validation of the DEGs (*Sparc*, *Adamts2*, *Pcolce2*, *Pcolce*, *Bmp1*, *Itga2*) from bulk RNA-seq analysis. For *Sparc*, $n = 4$ for shScramble-AAV injected group and $n = 6$ for sh*Wnt5a*-AAV injected group; for *Adamts2*, *Pcolce2* and *Bmp1*, $n = 5$ for both shScramble-AAV injected group and sh*Wnt5a*-AAV injected group; for *Pcolce*, $n = 3$ for shScramble-AAV injected group and $n = 5$ for sh*Wnt5a*-AAV injected group; for *Itga2*, $n = 4$ for shScramble-AAV injected group and $n = 5$ for sh*Wnt5a*-AAV injected group. One-way ANOVA with Bonferroni's post hoc test (two-sided) for *Sparc*, *Adamts2*, and *Pcolce*, Brown-Forsythe and Welch ANOVA tests with Dunnett's T3 post hoc tests (two-sided) for *Pcolce2*, *Bmp1*, and *Itga2*. **e**, **f** Network of the 20 hub genes and functional enrichment (one-sided hyper-geometric test with Benjamini–Hochberg correction for multiple testing) of the *Wnt5a* assigned gene module. **g** Western blots and densitometric quantification of scleral WNT5A and SAPRC proteins; representative blots are shown for sh*Wnt5a*-AAV injected mice. $n = 5$, Friedman tests with Dunn's post hoc test (two-sided) for WNT5A; RM-ANOVA with Bonferroni's post hoc test (two-sided) for SAPRC. **h**, **i** Immunofluorescence intensity and quantification of SPARC protein expression in the temporal/nasal iPPS, oPPS, and peripheral sclera of NC eyes. In FD-48h, $n = 6$ mic per group; in FD-2W, $n = 3$ for NC eyes and $n = 4$ for both FD-F and FD-T eyes. One-way ANOVA with Bonferroni's post hoc test (two-sided), Brown-Forsythe and Welch ANOVA tests with Dunnett's T3 post hoc test (two-sided) or Kruskal–Wallis non-parametric test with Dunn's post hoc test (two-sided) were used. Red: SPARC; blue: 4', 6-diamidino-2-phenylindole (DAPI); iPPS the inner peripapillary sclera, oPPS the outer peripapillary sclera, peripheral, the peripheral sclera. NC normal control eyes, FD-F untreated contralateral eyes of form deprivation mice, FD-T form deprivation treated eyes. Data are expressed as mean ± SEM.

equator, and finally reaching the posterior pole[51], It has been proposed that the gradient distribution of the scleral WNT5A concentration induces an asymmetric distribution of polar molecules within the cell through the activation of PCP signalling, This, in turn, affects cell polarity and directs scleral differentiation towards the posterior pole. However, the specific regulatory mechanism of action remains to be elucidated.

Wnt5a$^+$ fibroblasts exert their effects by modulating the scleral microenvironment through paracrine signalling by WNT5A, in addition to regulating their own function through autocrine signalling by WNT5A. For instance, *Wnt5a*$^+$ fibroblasts interact with Wnt receptor-expressing fibroblasts (e.g., *Comp*$^+$, *Fzd1*$^+$, *Igfbp2*$^+$) by secreting WNT5A. Consequently, interaction via the Wnt5a-receptor regulates the scleral ECM homeostasis and microenvironment.

A unique *Wnt5a*^{hi} fibroblast is involved in regulating the ECM by secreting WNT5A, and it affects the development of disease

The present study identified a novel fibroblast subtype characterised by high expression of *Wnt5a*. This particular subtype has been observed to mediate collagen synthesis and regulate ECM homeostasis; consequently, it has been designated '*Wnt5a*^{hi} fibroblast'. In addition, in our scRNA-seq data, scleral *Wnt5a*^{hi} fibroblasts have been shown to express elevated levels of *Cxcl5*, a chemokine that has been implicated in immune regulation, inflammatory response, and angiogenesis[52,53]. The *Wnt5a*$^+$ fibroblasts play a role in inflammation by inducing high levels of inflammatory factors (e.g. IL24)[54]. Therefore, it is suggested that *Wnt5a*^{hi} fibroblasts may be involved in myopia progression by controlling immune-inflammatory regulatory mechanisms in addition to directly regulating ECM homeostasis. Alterations in scleral inflammatory factors have also been reported in myopia progression, e.g. increases in IL6, IL8, TNFα, and C5a-9 in myopia[55,56]. Ccl2 is a cell chemokine that induces the secretion of MMP2 by macrophages in the sclera, promoting the development and progression of myopia[57]. Macrophages are also predominantly distributed in the posterior pole of the sclera, along with *Wnt5a*^{hi} fibroblasts; they overlap in spatial distribution. We observed that *Cxcl5* expression was significantly increased in *Wnt5a*^{hi} fibroblasts in form deprived eyes, which prompted us to hypothesise that the reduction of *Wnt5a*^{hi} fibroblasts has the potential to promote CXCL5 secretion, which in turn could stimulate macrophages to secrete collagen-degrading matrix metalloproteinases (e.g. MMP2). This would disrupt collagen synthesis and secretion, thereby reducing collagen levels and disrupting ECM homeostasis, and thus promoting myopia progression. Nevertheless, further investigation is required to elucidate the specific mechanism.

It was reported that *MMP/WNT5A*$^+$ fibroblasts increased at the lesion site in Crohn's disease[58], which is characterised by the presence of inflammation and fibrosis[59]. We speculated that elevations of *MMP/WNT5A*$^+$ fibroblasts at the lesion site upregulate WNT5A expression, which then activates the ncWnt pathway. This leads to overproduction of collagen synthesis and fibrotic pathological changes in intestinal tissues, ultimately promoting Crohn's disease. The number of *POSTN*$^+$*WNT5A*$^+$ cancer-associated fibroblast (CAF)-like fibroblasts increases in the skin of patients suffering from prurigo nodularis, which promotes cell adhesion and carcinogenesis via soluble WNT5A secretion[60]. It is hypothesised that *POSTN*$^+$*WNT5A*$^+$ fibroblasts increase at the lesion site, and the overproduction of WNT5A leads to an aberrant increase in collagen synthesis; this, in turn, causes local collagen deposition and cutaneous fibrosis, producing the characteristic nodules and thickened skin of prurigo nodularis.

In summary, we have identified a unique scleral fibroblast subtype that is directly involved in myopia development. Specifically, we observed a spatiotemporal expression pattern of scleral *Wnt5a*^{hi} fibroblasts, with cell density being highest in the posterior pole, which mediates the scleral responses to form deprivation myopia in murine eyes. Decreases in the number of scleral *Wnt5a*^{hi} fibroblasts inhibited the Wnt5a signalling pathway activation, which in turn disrupted the scleral microenvironment and impaired ECM homeostasis. As a result, COL1A1 expression levels declined, and this exacerbated myopia progression. These results broaden our understanding of the role of phenotypic heterogeneity of scleral fibroblasts in controlling ECM homeostasis and myopia onset and progression.

Methods

Animal care and ethics

The animal experiments were approved by the Animal Care and Ethics Committee at the Eye Hospital of Wenzhou Medical University (approval number: WYDW2020-0082). All experiments were conducted according to the Association for Research in Vision and Ophthalmology Statement for the Use of Animals in Ophthalmic and Visual Research.

Three-week-old C57BL/6 J, wild-type, male mice were purchased from Beijing Vital River Laboratory Animal Technology Co., Ltd. (Beijing, China). Only male mice were used, because sex-associated differences in eye growth have been reported in mice[61]. All animals were raised in standard transparent mouse cages in the Eye Hospital Animal Breeding Unit of Wenzhou Medical University. Food and water were available ad libitum. The diet was purchased from Jiangsu Xietong Pharmaceutical Bio-engineering Co., Ltd (Jiangsu, China; Cat# 1010058). A 12 h/12 h light/dark cycle (light from 8 a.m. to 8 p.m.) was provided by incandescent bulbs that produced an ambient luminance of approximately 300 lux on the cage floor. The room temperature was maintained at 22 ± 2 °C.

Induction of form-deprivation myopia and ocular biometric measurements in mice

Form deprivation myopia in mice was induced by covering the right eye of each animal with a handmade white translucent occluder.

https://doi.org/10.1038/s41467-025-67246-x

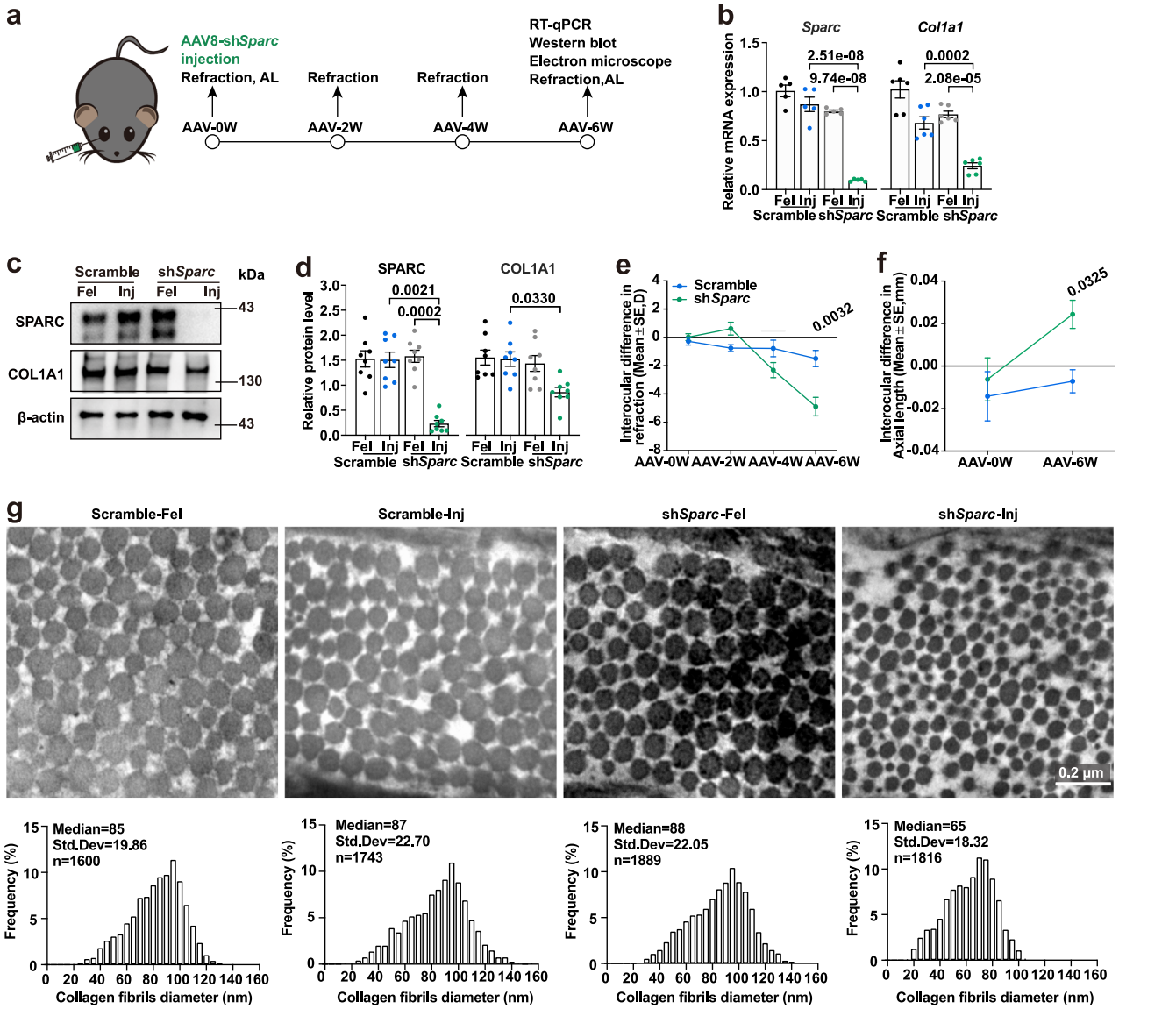

Fig. 7 | Changes in refraction, ocular biometrics in shScramble-AAV and sh*Sparc*-AAV injection in mice. a Schematic of the *shSparc*-AAV injection schedule. **b** Levels of *Sparc* and *Col1a1* mRNA were reduced after sub-Tenon's injection of sh*Sparc*-AAV. $n = 5$ for *Sparc* and $n = 6$ for *Col1a1*, one-way ANOVA with Bonferroni's post hoc test (two-sided). **c**, **d** Protein levels of SPARC and COL1A1 were reduced after sub-Tenon's injection of sh*Sparc*-AAV. $n = 8$, RM-ANOVA with Bonferroni's post hoc test (two-sided). **e** sh*Sparc*-AAV injected mice displayed a greater myopic shift than did the shScramble-AAV injected mice. $n = 12$, two-way repeated measures ANOVA with Bonferroni's post hoc test (two-sided). **f** Compared with the shScramble-AAV injected group, the sh*Sparc*-AAV injected group exhibited a significant increase in axial length. $n = 12$, two-way repeated measures ANOVA with Bonferroni's post hoc test (two-sided). **g** Scleral fibril ultrastructure of the fellow eye and the treated eyes in the shScramble-AAV injected mice, and in the sh*Sparc*-AAV injected mice ($n = 3$ mice per group). Data are expressed as mean ± SEM.

Briefly, the occluder was attached carefully to the fur around the eye with expanded polystyrene glue. A thin plastic collar was attached around the neck to prevent the removal of the occluder. Normal control (NC) mice were not fitted with an occluder and a plastic collar, but were completely untreated. Three-week-old C57BL/6 J mice were randomly divided into FD groups of 24 h, 48 h, and 2 weeks of treatment. Refraction and ocular biometric measurements of the FD-treated eyes (FD-T), FD-fellow eyes (FD-F), and NC eyes were obtained before and at the end of the 2 weeks of each treatment group.

An eccentric infra-red photoretinoscope was used to measure ocular refraction of unanesthetized mice in a dark room[62,63]. In brief, each mouse was positioned on a platform in front of the photoretinoscope, and the data were recorded when the Purkinje image appeared in the centre of the pupil[64]. All measurements were repeated at least three times for each eye. Ocular biometrics, including corneal thickness, anterior chamber depth, lens thickness, vitreous chamber depth, corneal radius of curvature, and axial length (AL), were measured with a custom-built real-time optical coherence tomography (OCT) instrument, described in detail elsewhere[65]. The data were recorded and analysed with custom-designed software as previously described[65]. Each measurement was replicated three times in each eye, and the average value was used.

Scleral single-cell RNA sequencing (scRNA-Seq) of FDM mice

Preparation of scleral single-cell suspensions. After 24 and 48 h of FD treatment, the mice were asphyxiated with CO_2 and sacrificed by cervical dislocation. The eyes were then enucleated and dissected under a stereomicroscope to obtain the sclera. To obtain enough cells for single-cell analysis, eight sclerae were pooled to form a single sample. The sclera was cut into small pieces and subjected to enzymatic digestion in a solution containing 1.5 mg/mL collagenase I (#C0131, Sigma Aldrich, St. Louis, MO, USA), collagenase IV (#17104-

https://doi.org/10.1038/s41467-025-67246-x

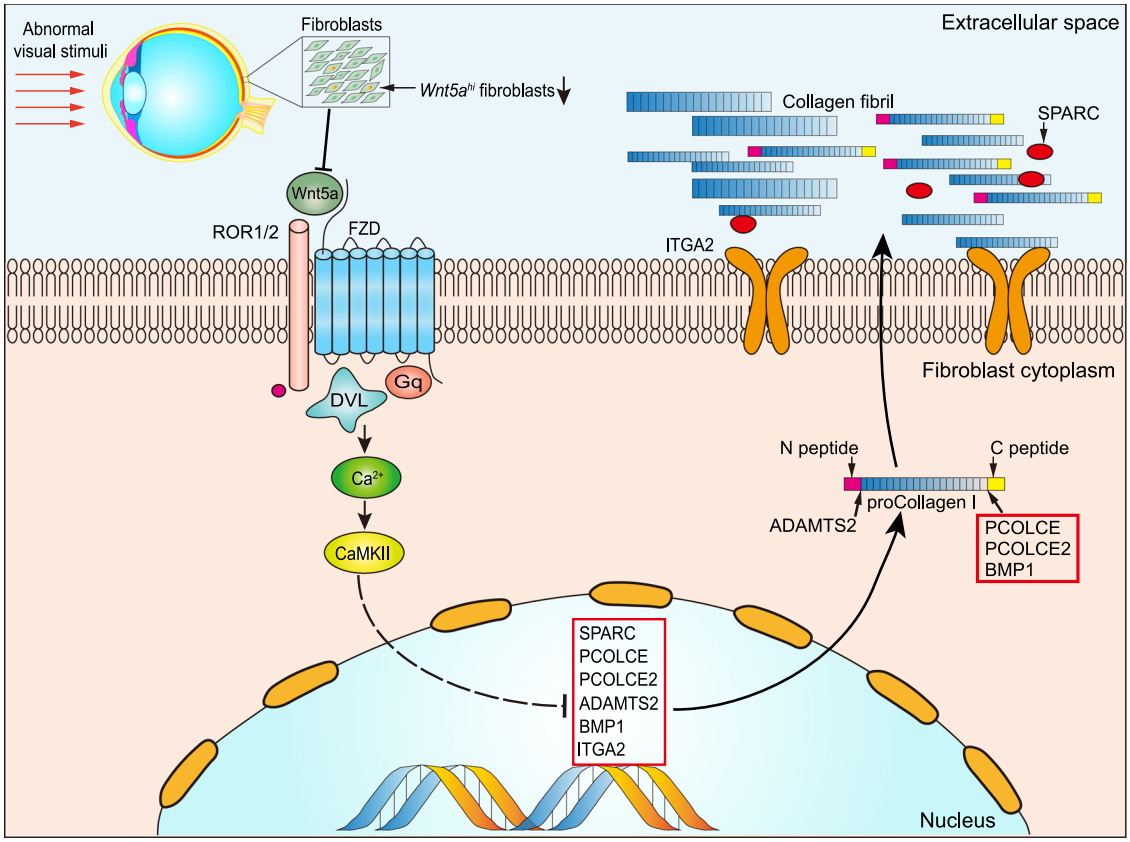

Fig. 8 | A paradigm for *Wnt5a*^{hi} fibroblast involvement in the scleral ECM homeostasis and pathogenesis of myopia. Abnormal visual stimulation propagating via the retina-choroid-sclera signalling cascade reduces *Wnt5a*^{hi} fibroblast numbers and/or activity, and thus Wnt5a secretion. Subsequently, the expression of genes for ECM molecules such as *Col1a1*, *Sparc*, *Pcolce*, *Pcelce2*, *Adamts2*, *Bmp1*, and *Igta2* is downregulated via the noncanonical Wnt signalling pathway (Wnt5a-Ca^{2+}-CaMKII). This response may disrupt ECM structural organisation, decrease collagen I level, and reduce the collagen fibril diameter, finally resulting in myopia progression due to increased distension of the posterior sclera under constant intraocular pressure.

019, Gibco BRL, Grand Island, NY, USA), and 0.2% (wt/vol) trypsin (#27250-018, Gibco) for 1 h at 37 °C in a thermostatic incubator. Subsequently, the reaction was neutralised in a solution with 10% foetal bovine serum (#10099141c, Gibco) and 0.02% ethylenediaminetetraacetic acid (EDTA) (#E8008, Sigma Aldrich). The scleral tissue was dissociated gently using a 200 µL pipette tip to generate a single-cell suspension. The dissociated scleral cells were subjected to a series of steps: washing, pelleting, resuspension, and filtration through a 40 µm nylon cell strainer (#352340, Corning Inc., Corning, NY, USA) to eliminate all clumped cells. The isolated single-cell suspensions were then diluted in 0.5% MACS bovine serum albumin (BSA) Stock Solution (#130091376, Miltenyi Biotec, Bergisch Gladbach, Germany) to achieve an average concentration of 1000 cells/µL for subsequent use.

scRNA-seq. scRNA-seq was conducted at Novogene Co., Ltd. (Beijing, China). After FD for each of the two durations (FD-24 h and FD-48 h), four pooled scleral samples were assayed (two from FD-treated eyes and two from FD-fellow eyes), yielding 8 samples. The digested single cells of those samples were partitioned into Gel Bead-in-Emulsions and barcoded in cDNA libraries using the Chromium Single Cell 3′ GEM, Library & Gel Bead Kit (V3, 10× Genomics, Pleasanton, CA, USA) following the instructions set out in the user manual. The single-cell libraries were sequenced in a 150 bp paired-end configuration using Illumina NovaSeq 6000 (San Diego, CA, USA).

Bioinformatic analysis of scRNA-seq

scRNA-seq data processing. Sequencing data alignment and gene expression matrix calculations were performed with Cell Ranger 5.0.1 (10× Genomics, San Francisco, CA, USA). A pre-built mouse reference genome, based on mouse reference build 38 and mouse gene annotation version 23 (Ensembl 98), was downloaded from the 10× Genomics website. Cells with a percentage of mitochondrial genes >25%, expressed genes <100 or >5000, and estimated as doublets by the scds package were removed from further analysis[66].

Batch effect removal, dimension reduction, clustering, and cell type annotation

The Seurat package (version 4.1.1) was adopted for batch effect removal, dimension reduction, and unsupervised cell clustering[67]. Before processing, the mitochondrial and ribosomal genes were removed. The SCTransform module was used for batch effect correction[68]. The cell cycle score calculated by the CellCycleScoring module of Seurat, the percentage of mitochondrial genes, and the number of expressed genes were used as variables to regress out for the batch effect removal process. The 3000 most variable genes were selected for integrating data from different batches and for principal component (PC) analysis. The first 30 PCs were used for identifying cell clusters with a resolution of 0.3. Clustering results were illustrated in uniform manifold approximation and projection (UMAP) space.

The SingleR package was used for defining the cell type according to their similarity to mouse RNA-seq data of the celldex package[69]. Clusters were assigned to cell types according to the SingleR results of the majority of cells in the corresponding clusters. The annotation results were adjusted according to known cell type-specific markers, including muscle cells, keratocytes, retinal pigment epithelial cells and Schwann cells, to obtain the final results.

Fibroblasts subtype analysis

Clusters of cells that were defined as fibroblasts were extracted for fibroblast subtype analysis. Extracted cells with the original SingleR annotation as non-fibroblasts were removed from further analysis. The sub-clustering resolution was defined as 0.4, from which the *Pi16*$^+$ cells (a universal fibroblast subcluster) can form an independent cluster.

The pan-tissue fibroblast data were obtained from the original research[23]. Scleral fibroblasts were combined with pan-tissue using the FindIntegrationAnchor function of Seurat. The 3000 most variable genes and the top 30 PCs were used for clustering with a resolution of 0.1.

Marker genes were defined as expressed in more than 40% of cells in the corresponding cluster, and a percentage difference of more than 20% between the corresponding cluster and the remaining cells. Scleral fibroblast subtypes were defined by the marker genes.

Cell–cell communications were conducted with the CellChat package[70]. 'Secreted Signalling' or 'ECM-Receptor' of ligand-receptor interactions was selected for building the communication network in mice. Differences in information flow in each interaction-signalling pathway between FD-treated and fellow sclerae were calculated by the 'rankNet' function, and the paired Wilcoxon test was adopted to identify the significant differences in the flow of signalling information between these two conditions.

Weighted gene co-expression network analysis of scRNA-seq data was performed by the hdWGCNA R package[71]. Genes expressed in at least 5% of each cell type were selected for network construction. Cells were combined into meta cells according to cell types and treatment groups. The soft-power threshold was selected automatically with a scale-free topology model fit with a cutoff of 0.8 in a signed network type. After the construction of the co-expression network, module eigengenes were calculated using the treatment group as the covariant. Module hub genes were set as the top 20 genes with the highest module eigengene-based connectivity (kME) score. Differential module eigengene analysis between treatment groups was performed by the Find DMEs function of the hdWGCNA R package.

RNA FISH

RNA was detected in sections of murine sclera using the RNAscope Multiplex Fluorescent Reagent Kit v2 Assay (#323100, ACD Bio, Minneapolis, MN, USA), according to the manufacturer's instructions. In brief, the slides were initially rinsed three times for 5 min in phosphate-buffered saline (PBS). Subsequently, the sections were left to dry for 5 min before incubation in 5 drops of RNAscope Hydrogen Peroxide for 10 min. Following this, the sections were rinsed again with distilled water. Antigen retrieval was conducted by incubating the slides for 5 min in RNAscope Target Retrieval Reagent (#322000, ACD Bio) at 100 °C. The slides were subsequently rinsed in distilled water and then incubated for 3 min in 100% ethanol. Subsequently, the slides were incubated with five drops of Protease III for 30 min at 40 °C in the ACD HybEZ II Hybridisation System (#321720, ACD Bio). Following this incubation period, the slides were washed with distilled water. The RNAscope probes, *A2m*-C1 (#853411, ACD Bio) and *Wnt5a*-C2 (#316791-C2, ACD Bio), Positive Control Probe (#320881, ACD Bio), and Negative Control Probe (#320871, ACD Bio) were then hybridised for 2 h at 40 °C, after which they were amplified in accordance with the manufacturer's instructions. Following counterstaining with DAPI, images were captured using a Zeiss 880 confocal laser microscope (Carl Zeiss Microimaging GmbH, Jena, Germany) with a Plan-Apochromat 20×/0.8 NA objective, except for the high-magnification views in the *Wnt5a*$^+$ fibroblast validation (for display purposes only), which were acquired using a Plan-Apochromat 63×/1.4 NA oil immersion DIC objective. Following the previous description[72], the scleral portion was divided into inner peripapillary sclera (iPPS), outer peripapillary sclera (oPPS), and peripheral sclera, in a subsequent analysis using Fiji software (FIJI Is Just ImageJ, version 2.14). For each eye and each predefined anatomical location, three non-overlapping fields of view were imaged and analysed. The number of *Wnt5a*$^+$ cells and the percentage of *Wnt5a*$^+$ cells that were scleral fibroblasts were analysed. To eliminate subjective bias in identifying cells as *Wnt5a*$^+$ without the use of a cytoplasmic or cell membrane marker, we further analysed the number of all spots in the whole image and defined the outcome measure as spots/1000 μm^2.

Gene expression analysis with RT-qPCR

Total scleral RNA was isolated using the RNeasy Fibrous Tissue Mini Kit (#74704, Qiagen, GmbH, Hilden, Germany), and its purity was assessed using a Nanodrop (Thermo Fisher Scientific, Waltham, MA, USA). A total of 200 ng of RNA was reverse transcribed to cDNA using the rtStar First-Strand cDNA Synthesis Kit (#AS-FS-003-02, Arraystar, Rockville, MD, USA) with an $A_{260/A280}$ ratio of 1.8–2.0. Subsequently, reverse-transcription quantitative polymerase chain reaction (RT-qPCR) was performed. The reaction mixture was analysed using a QuantStudio 6 Flex System or a ViiA 7 Real-Time PCR system (Applied Biosystems, Carlsbad, CA, USA) with a Power SYBR Green PCR Master Mix (#4367659, Applied Biosystems), following the manufacturer's instructions. The following conditions were employed for the PCR: The reaction was initiated at 50 °C for 2 min and 95 °C for 10 min, followed by 40 cycles of amplification at 95 °C for 15 s and 60 °C for 60 s. Melting curve analysis was employed to ascertain the specific amplification. The specific gene products were amplified using the primer pairs listed in Supplementary Table 1. mRNA expression levels were analysed using the comparative $2^{-\Delta\Delta}$Ct method and normalised using β-actin (*Actb*) as the reference standard.

Immunofluorescence

Following 48 h or 2 weeks of FD, all C57BL/6 J mice were euthanised using CO_2 asphyxiation. The eyes were enucleated and bisected through the equatorial plane, creating posterior segment eyecups, which were fixed in 4% paraformaldehyde in 0.1 M phosphate-buffered saline (PBS), pH 7.4, for 30 min at room temperature; Subsequently the eyecups were immersed in 10% and then 20% sucrose, for 2 h each, and finally in 30% sucrose for 24 h at 4 °C. The eyecups were embedded in an optimal cutting temperature compound (OCT; Thermo Fisher Scientific), followed by rapid freezing in liquid nitrogen. The samples were sectioned at a thickness of 10 µm using a cryostat microtome. The sections were blocked with 6% normal donkey serum, 1% BSA, and 0.2% Triton X-100 in 0.1 M PBS for 2 h at room temperature, then incubated with rabbit polyclonal antibodies against WNT5A (1:100, #bs-1948R, Bioss, Woburn, MA, USA) and SPARC (1:300, #15274-1-AP, Proteintech, Rosemont, IL, USA) for 24 h at 4 °C. Following a wash with PBS, the sections were incubated with donkey anti-rabbit IgG (H + L) secondary antibody, Alexa Fluor 488 (#A21206, Thermo Fisher Scientific), or donkey anti-rabbit IgG (H + L) secondary antibody, Alexa Fluor 555 (#A31572, Thermo Fisher Scientific), respectively, for 2 h at room temperature. The nuclei were stained with 4′, 6-diamidino-2-phenylindole (DAPI, #P0131, Beyotime Biotechnology, Shanghai, China) for 5 min, followed by mounting with phenylenediamine to stain lipids. The sections were viewed using a Zeiss 880 microscope (Carl Zeiss Microimaging GmbH) with a Plan-Apochromat 20×/0.8 NA objective lens.

Western blotting

The HSFs and murine sclerae were lysed in SDS Lysis buffer (#P0013G, Beyotime Biotechnology), which was supplemented with Complete Mini (a protease inhibitor cocktail), 1 mM phenylmethylsulfonyl fluoride (PMSF, #ST506, Beyotime Biotechnology), and 1 mM DL-dithiothreitol (#D0632, Sigma Aldrich). Samples containing an equal weight of protein (20 µg) were loaded onto

4–12% FuturePAGE gel (#ET15412Gel, ACE Biotechnology, Changzhou, China), separated by electrophoresis, and subsequently transferred onto a nitrocellulose membrane (#HATF00010, Millipore, Billerica, MA, USA). Following a 2 h incubation period at room temperature with 5% non-fat milk, the membranes were incubated with primary antibodies overnight at 4 °C. The membranes were washed three times with TBST (tris-buffered saline with 1% Tween-20), then probed with dilution 1:10000 goat anti-rabbit IgG (H + L) secondary antibody conjugated to HRP (#31460, Invitrogen Life Technologies, Carlsbad, CA, USA) or goat anti-mouse IgG (H + L) secondary antibody-HRP (#31430, Invitrogen Life Technologies) for 2 h at room temperature. The membranes were again washed three times with TBST, followed by visualisation using the electrochemiluminescence software. Finally, the protein bands were quantified by densitometric analysis with ImageJ software (version 1.53a, NIH, Bethesda, MD, USA). Primary antibodies were targeted to WNT5A (1:1000; #2392S, Cell Signalling Technology, Beverly, MA, USA), SPARC (in vivo: 1:1000, #ab290636, Abcam, Cambridge, MA, USA; in vitro: 1:1000, #15274-1-AP, Proteintech), COL1A1 (1:1000, #67288-1-Ig, Proteintech), α-SMA (1:1000, #ab7817, Abcam), MMP2 (1:3000; #10373-2-AP, Proteintech), β-Catenin (1:2000; #17565-1-AP, Proteintech), p-CaMK2 (1:1000; #12716, Cell Signalling Technology), CaMK2 (1:1000; #4436S, Cell Signalling Technology), β-actin (1:1000; #66009-1-Ig, Proteintech), or α-tubulin (1:2000; #66031-1-Ig, Proteintech).

Scleral bulk RNA sequencing

After sub-Tenon's injection of sh*Wnt5a*-AAV for 6 weeks, the mice were asphyxiated with CO_2 and sacrificed. The sclera was dissected out of the enucleated eyes, and seven sclerae were pooled together to form one sample because of their low RNA content. The total RNA was extracted using a RNeasy Fibrous Tissue Mini Kit (#74704, Qiagen, GmbH, Hilden, Germany). RNA sequencing was conducted at Cloud-seq (Cloud Sequence Biotech Co., Ltd., Shanghai, China). Briefly, sequencing libraries were produced using the NEBNext Ultra II Directional RNA Library Prep Kit (New England Biolabs, Inc., Massachusetts, USA) according to the manufacturer's instructions. The libraries were sequenced on an Illumina HiSeq 4000 platform with 150 bp paired-end reads. The sequencing reads were aligned to the mouse reference genome build 38 (GRCm38)/mm10 by STAR 2.7.0. The expression matrix was obtained by subreads 2.0.3. Differentially expressed analysis was performed by DESeq2 1.48.0.

Sub-Tenon's capsule injection of sh*Wnt5a*-AAV, sh*Sparc*-AAV or *Wnt5a*-AAV overexpression in mice

The shRNA plasmid (pAAV-U6-sh*Wnt5a*-CMV-EGFP-WPRE, pAAV-U6-sh*Sparc*-CMV-EGFP- WPRE) was used to interfere with *Wnt5a*, while pAAV-U6-shNC (Scramble sequences)-CMV- EGFP-WPRE) served as the negative control. The plasmid (pAAV-CMV-*Wnt5a*-3×FLAG-P2A-mNeonGreen-tWPA) was used to overexpress *Wnt5a*, while pAAV-CMV-3×FLAG-P2A- mNeonGreen-tWPA empty vector served as the negative control. These plasmids were packaged with adeno-associated virus (AAV)2/8 serotype at OBiO (OBiO Biotechnology Co., Ltd., Shanghai, China) for infection. Three-week-old C57BL/6 J mice were deeply anaesthetised using isoflurane. A 33-gauge, Small Hub RN Needle (#7803-05, Hamilton Company, Switzerland) was front-loaded with 8 µL AAV solution (1×10^{13} viral particles/ml). The needle was carefully inserted into Tenon's capsule, at an angle of approximately 30 degrees (relative to the scleral surface), and 14–18 mm away from the corneal limbus. Eyes were covered with 0.2% polyacrylic acid every day for 3 days after the AAV injection.

Transmission electron microscopy

Tissue buttons, 0.5 × 1.0 mm in size, containing choroid and sclera were punched out 0.5 mm away from the temporal margin of the optic disc and processed for transmission electron microscopy as described previously[73,74]. Cross-sections were visualised using a Hitachi H-7500 transmission electron microscope (Hitachi, Tokyo, Japan). Serial sections from the centre of each block were measured to ensure that the analysis was performed in the designated sectioning positions in each layer, as well as at the same depth. Three electron micrographs taken randomly from the middle layers of the sclera in each eye at ×30,000 magnification.

The diameter of the fibrils was measured using Fiji software. The statistical analysis of fibril diameters was conducted as previously described[73,74]. To eliminate any potential confounding effects of differences in fibril number on the shape of the histogram, a percentage frequency histogram was utilised in the analysis. To ascertain the distribution of fibril diameters, the median was represented, which shows the location of the centre of the distribution. The estimation of the mean density of the scleral fibrils was based on the number of fibril cross-sections in a randomly selected area in each micrograph.

siRNA-mediated *WNT5A* and *SPARC* knockdown in HSFs

The use of the donor eyeball complied with the tenets of the Declaration of Helsinki for Research Involving Human Tissue and was approved by the Ethics Committee at the Eye Hospital of Wenzhou Medical University in China (approval number: Y2017-039). The donor had signed permission to 'voluntarily donate the eyeballs after death' for organ transplantation and medical research. The primary human scleral fibroblasts (HSFs) were isolated from the donor (male, 38 years, Han ethnicity) eyeball as previously described[75]. In brief, the donor eyeball was enucleated within 4 h of death, and the cornea were extracted for corneal transplantation. The sclera was then separated from the other ocular tissues and chipped into 1 × 1 mm pieces. These pieces were then attached to the culture dish and incubated in Dulbecco's modified Eagle's medium (DMEM, Gibco, Grand Island, NY, USA) supplemented with 10% (v/v) foetal bovine serum (FBS, Gibco) and 1% GlutaMAX™-I (Gibco) and maintained in a 5% CO2, 95% O2 air humidified incubator at 37 °C. After the primary culture reached confluence, the cells were detached using a 0.05% trypsin/0.02% EDTA solution. After dilution to 1:2 to 1:3 ratios, the cells were seeded into 25 cm^2 flasks for subculture, establishing the cell lines. The cultured cells were unresponsive to labelling with anticytokeratin, confirming the purity of the scleral fibroblasts. The scleral fibroblasts in cell lines (passages 8–10) were used in this study. The HSFs in the logarithmic growth phase were seeded on a 12 or 24-well tissue culture plate.

To analyse the contribution of *WNT5A* or SPARC to scleral ECM, we determined the effect of its downregulation on COL1A1, MMP2, and α-SMA levels in the HSFs. The HSFs were transfected with siRNA (50 nM) by using Lipofectamine RNAiMAX (Thermo Fisher Scientific) according to the typical RNAiMAX transfection procedure. We used the following human *WNT5A* siRNA oligos: si*WNT5A*: 5′-CGCCCAGGTTGTAATTGAA-3′, si*SPARC1*: 5′-GACTTCGAGAAGAAC TATA-3′; and si*SPARC2*: ATCGACAAGGATCTTGTGA (RiboBio Co. Ltd, Guangzhou, China). In all experiments, a validated scrambled sequence (RiboBio) was used as the negative control, only with the supplied transfection reagents, which served as the mock condition. Western blot analysis of the WNT5A or SPARC protein levels was performed to determine the knockdown efficiency of si*WNT5A or* si*SPARC*. The effects of *WNT5A* or *SPARC* knockdown on COL1A1, MMP2, α-SMA, p-CaMK2, p-CaMK2, and β-catenin protein levels were also evaluated with Western blot analysis.

Statistics

Descriptive statistics and data analysis were performed using GraphPad Prism software (Version 9.0.0; GraphPad Inc., San Diego, CA, USA). Data were expressed as mean ± standard error of the mean. Normality and homogeneity of variances for each treatment group were determined by Shapiro-Wilk tests. Depending upon whether the samples

being compared met the criteria of normal distributions and equal variances. For independent samples, multiple comparisons were analysed by one-way analysis of variance (ANOVA) with Bonferroni's post hoc tests, or Kruskal-Wallis non-parametric tests with Dunn's post hoc tests, respectively; and if the assumption of equal variances was violated, Brown-Forsythe and Welch ANOVA tests with Dunnett's T3 post hoc tests were used. As for matched samples, multiple comparisons were conducted using repeated measures analysis of variance (RM-ANOVA) with Bonferroni's post hoc test, or the Friedman test with Dunn's post hoc test. Two-way repeated measures ANOVA with Bonferroni's post hoc test was used to analyse changes over time. Differences were defined as significant at values of P less than 0.05.

Reporting summary

Further information on research design is available in the Nature Portfolio Reporting Summary linked to this article.

Data availability

The raw sequence data of single cell and bulk tissue RNA sequencing of mouse sclera used in this paper have been deposited in the Genome Sequence Archive in the National Genomics Data Centre, China National Centre for Bioinformation (GSA: CRA025141) are publicly accessible at https://ngdc.cncb.ac.cn/gsa/browse/CRA025141. The single cell RNA sequencing data of human sclera used in this paper were obtained from the Single Cell Portal of the BROAD Institute under the accession SCP2298. Source data are provided with this paper.

References

1. Holden, B. A. et al. Global Prevalence of Myopia and High Myopia and Temporal Trends from 2000 through 2050. *Ophthalmology* **123**, 1036–1042 (2016).
2. Dolgin, E. The myopia boom. *Nature* **519**, 276–278 (2015).
3. Nakao, S. Y. et al. Myopia prevalence and ocular biometry features in a general japanese population: the nagahama study. *Ophthalmology* **128**, 522–531 (2021).
4. Cho, B. J., Shin, J. Y. & Yu, H. G. Complications of pathologic myopia. *Eye Contact Lens* **42**, 9–15 (2016).
5. Baird, P. N. et al. Myopia. *Nat. Rev. Dis. Prim.* **6**, 99 (2020).
6. Rada, J. A., Shelton, S. & Norton, T. T. The sclera and myopia. *Exp. Eye Res.* **82**, 185–200 (2006).
7. McBrien, N. A. Gentle A. role of the sclera in the development and pathological complications of myopia. *Prog. Retin Eye Res.* **22**, 307–338 (2003).
8. Gentle, A., Liu, Y., Martin, J. E., Conti, G. L. & McBrien, N. A. Collagen gene expression and the altered accumulation of scleral collagen during the development of high myopia. *J. Biol. Chem.* **278**, 16587–16594 (2003).
9. Keeley, F. W., Morin, J. D. & Vesely, S. Characterization of collagen from normal human sclera. *Exp. Eye Res.* **39**, 533–542 (1984).
10. McBrien, N. A., Jobling, A. I. & Gentle, A. Biomechanics of the sclera in myopia: extracellular and cellular factors. *Optom. Vis. Sci.* **86**, E23–E30 (2009).
11. Wu, W. et al. Hypoxia-induced scleral HIF-2α upregulation contributes to rises in MMP-2 expression and myopia development in mice. *Invest Ophthalmol. Vis. Sci.* **63**, 2 (2022).
12. Zhao, F. et al. Cause and effect relationship between changes in scleral matrix metallopeptidase-2 expression and myopia development in mice. *Am. J. Pathol.* **188**, 1754–1767 (2018).
13. Liu, H. H., Kenning, M. S., Jobling, A. I., McBrien, N. A. & Gentle, A. Reduced scleral TIMP-2 expression is associated with myopia development: TIMP-2 supplementation stabilizes scleral biomarkers of myopia and limits myopia development. *Investig. Ophthalmol. Vis. Sci.* **58**, 1971–1981 (2017).
14. Boyd, D. F. et al. Exuberant fibroblast activity compromises lung function via ADAMTS4. *Nature* **587**, 466–471 (2020).
15. Nakahara, Y. et al. Fibroblasts positive for meflin have anti-fibrotic properties in pulmonary fibrosis. *Eur. Respir. J.* **58**, 2003397 (2021).
16. Li W et al. Single-cell RNA-seq of heart reveals intercellular communication drivers of myocardial fibrosis in diabetic cardiomyopathy. *Elife* **12**, e80479 (2023).
17. Huang, X., Wang, L., Guo, H., Zhang, W. & Shao, Z. Single-cell transcriptomics reveals the regulative roles of cancer associated fibroblasts in tumor immune microenvironment of recurrent osteosarcoma. *Theranostics* **12**, 5877–5887 (2022).
18. Phan, Q. M., Sinha, S., Biernaskie, J. & Driskell, R. R. Single-cell transcriptomic analysis of small and large wounds reveals the distinct spatial organization of regenerative fibroblasts. *Exp. Dermatol.* **30**, 92–101 (2021).
19. Wu, H. et al. Scleral hypoxia is a target for myopia control. *Proc. Natl. Acad. Sci. USA* **115**, E7091–E7100 (2018).
20. Plikus, M. V. et al. Fibroblasts: origins, definitions, and functions in health and disease. *Cell* **184**, 3852–3872 (2021).
21. Monavarfeshani, A. et al. Transcriptomic analysis of the ocular posterior segment completes a cell atlas of the human eye. *Proc. Natl. Acad. Sci. USA* **120**, e2306153120 (2023).
22. Jovic, D. et al. Single-cell RNA sequencing technologies and applications: a brief overview. *Clin. Transl. Med.* **12**, e694 (2022).
23. Buechler, M. B. et al. Cross-tissue organization of the fibroblast lineage. *Nature* **593**, 575–579 (2021).
24. Jin, Y. et al. Wnt5a attenuates hypoxia-induced pulmonary arteriolar remodeling and right ventricular hypertrophy in mice. *Exp. Biol. Med.* **240**, 1742–1751 (2015).
25. Harada, A. et al. Hypoxia-induced Wnt5a-secreting fibroblasts promote colon cancer progression. *Nat. Commun.* **16**, 3653 (2025).
26. Wu, W. et al. Hypoxia-Induced Scleral HIF-2alpha upregulation contributes to rises in MMP-2 expression and myopia development in mice. *Investig. Ophthalmol. Vis. Sci.* **63**, 2 (2022).
27. Serra, R., Easter, S. L., Jiang, W. & Baxley, S. E. Wnt5a as an effector of TGFbeta in mammary development and cancer. *J. Mammary Gland Biol. Neoplasia* **16**, 157–167 (2011).
28. Newman, D. R. et al. Expression of WNT5A in idiopathic pulmonary fibrosis and its control by TGF-beta and WNT7B in human lung fibroblasts. *J. Histochem. Cytochem.* **64**, 99–111 (2016).
29. Ku, H. et al. The role of transforming growth factor beta in myopia development. *Mol. Immunol.* **167**, 34–42 (2024).
30. Jiao, S. et al. Calcipotriol attenuates form deprivation myopia through a signaling pathway parallel to TGF-beta2-induced increases in collagen expression. *Investig. Ophthalmol. Vis. Sci.* **64**, 2 (2023).
31. Sergi, C. M. The role of SPARC/ON in human osteosarcoma. *Adv. Protein Chem. Struct. Biol.* **133**, 181–192 (2023).
32. Conforti, F. et al. Paracrine SPARC signaling dysregulates alveolar epithelial barrier integrity and function in lung fibrosis. *Cell Death Discov.* **6**, 54 (2020).
33. Gao, H., Frost, M. R., Siegwart, J. T. Jr. & Norton, T. T. Patterns of mRNA and protein expression during minus-lens compensation and recovery in tree shrew sclera. *Mol. Vis.* **17**, 903–919 (2011).
34. Guo, L., Frost, M. R., Siegwart, J. T. Jr & Norton, T. T. Scleral gene expression during recovery from myopia compared with expression during myopia development in tree shrew. *Mol. Vis.* **20**, 1643–1659 (2014).
35. Guo, L., Frost, M. R., Siegwart, J. T. Jr & Norton, T. T. Gene expression signatures in tree shrew sclera during recovery from minus-lens wear and during plus-lens wear. *Mol. Vis.* **25**, 311–328 (2019).
36. Li, X. J. et al. Posterior scleral reinforcement combined with vitrectomy for myopic foveoschisis. *Int J. Ophthalmol.* **9**, 258–261 (2016).
37. Miyake, M. et al. Identification of myopia-associated WNT7B polymorphisms provides insights into the mechanism underlying the development of myopia. *Nat. Commun.* **6**, 6689 (2015).

38. Fan, B. J. et al. Family-based genome-wide association study of south indian pedigrees supports WNT7B as a central corneal thickness locus. *Invest Ophthalmol. Vis. Sci.* **59**, 2495–2502 (2018).
39. Ma, M. et al. Wnt signaling in form deprivation myopia of the mice retina. *PLoS ONE* **9**, e91086 (2014).
40. Liu, Z. et al. Canonical Wnt signaling drives myopia development and can be pharmacologically modulated. *Investig. Ophthalmol. Vis. Sci.* **62**, 21 (2021).
41. Hu, S., Ouyang, S., Liu, H., Zhang, D. & Deng, Z. The effect of Wnt/beta-catenin pathway on the scleral remolding in the mouse during form deprivation. *Int Ophthalmol.* **41**, 3099–3107 (2021).
42. Li, M. et al. Expression of Wnt/beta-catenin signaling pathway and its regulatory role in type I collagen with TGF-beta1 in scleral fibroblasts from an experimentally induced myopia guinea pig model. *J. Ophthalmol.* **2016**, 5126560 (2016).
43. Suo, N. C. et al. Effects of latanoprost on the expression of TGF-beta1 and Wnt / beta-catenin signaling pathway in the choroid of form-deprivation myopia rats. *Cell Mol. Biol.* **66**, 71–75 (2020).
44. Hysi, P. G. et al. Meta-analysis of 542,934 subjects of European ancestry identifies new genes and mechanisms predisposing to refractive error and myopia. *Nat. Genet.* **52**, 401–407 (2020).
45. Wang, C., Xie, Y. & Wang, G. The elastic modulus and collagen of sclera increase during the early growth process. *J. Mech. Behav. Biomed. Mater.* **77**, 566–571 (2018).
46. Desgrange A, Le Garrec JF, Meilhac SM. Left-right asymmetry in heart development and disease: forming the right loop. *Development* **145**, dev162776 (2018).
47. Torban, E. & Sokol, S. Y. Planar cell polarity pathway in kidney development, function and disease. *Nat. Rev. Nephrol.* **17**, 369–385 (2021).
48. Zhang, K. et al. Wnt5a-Vangl1/2 signaling regulates the position and direction of lung branching through the cytoskeleton and focal adhesions. *PLoS Biol.* **20**, e3001759 (2022).
49. Andre, P., Song, H., Kim, W., Kispert, A. & Yang, Y. Wnt5a and Wnt11 regulate mammalian anterior-posterior axis elongation. *Development* **142**, 1516–1527 (2015).
50. Witze, E. S., Litman, E. S., Argast, G. M., Moon, R. T. & Ahn, N. G. Wnt5a control of cell polarity and directional movement by polarized redistribution of adhesion receptors. *Science* **320**, 365–369 (2008).
51. Sellheyer, K. & Spitznas, M. Development of the human sclera. A morphological study. *Graefes Arch. Clin. Exp. Ophthalmol.* **226**, 89–100 (1988).
52. Yin, C. et al. CXCL5 activates CXCR2 in nociceptive sensory neurons to drive joint pain and inflammation in experimental gouty arthritis. *Nat. Commun.* **15**, 3263 (2024).
53. Chen, C., Lin, L. Y., Chen, J. W. & Chang, T. T. CXCL5 suppression recovers neovascularization and accelerates wound healing in diabetes mellitus. *Cardiovasc. Diabetol.* **22**, 172 (2023).
54. Francis, L. et al. Single-cell analysis of psoriasis resolution demonstrates an inflammatory fibroblast state targeted by IL-23 blockade. *Nat. Commun.* **15**, 913 (2024).
55. Xu, R., Zheng, J., Liu, L. & Zhang, W. Effects of inflammation on myopia: evidence and potential mechanisms. *Front. Immunol.* **14**, 1260592 (2023).
56. Gao, T. T., Long, Q. & Yang, X. Complement factors C1q, C3 and C5b-9 in the posterior sclera of guinea pigs with negative lens-defocused myopia. *Int J. Ophthalmol.* **8**, 675–680 (2015).
57. Zhao, F. et al. Up-regulation of matrix metalloproteinase-2 by scleral monocyte-derived macrophages contributes to myopia development. *Am. J. Pathol.* **190**, 1888–1908 (2020).
58. Mukherjee, P. K. et al. Stricturing Crohn's disease single-cell RNA sequencing reveals fibroblast heterogeneity and intercellular interactions. *Gastroenterology* **165**, 1180–1196 (2023).
59. Alfredsson, J. & Wick, M. J. Mechanism of fibrosis and stricture formation in Crohn's disease. *Scand. J. Immunol.* **92**, e12990 (2020).
60. Patel, J. R. et al. Single-cell RNA sequencing reveals dysregulated POSTN+WNT5A+ fibroblast subclusters in prurigo nodularis. *J. Investig. Dermatol.* **144**, 1568–1578 e1565 (2024).
61. Barathi, V. A., Boopathi, V. G., Yap, E. P. & Beuerman, R. W. Two models of experimental myopia in the mouse. *Vis. Res.* **48**, 904–916 (2008).
62. Zhou, X. et al. The development of the refractive status and ocular growth in C57BL/6 mice. *Investig. Ophthalmol. Vis. Sci.* **49**, 5208–5214 (2008).
63. Huang, F. et al. Dopamine D1 receptors contribute critically to the apomorphine-induced inhibition of form-deprivation myopia in mice. *Investig. Ophthalmol. Vis. Sci.* **59**, 2623–2634 (2018).
64. Schaeffel, F., Burkhardt, E., Howland, H. C. & Williams, R. W. Measurement of refractive state and deprivation myopia in two strains of mice. *Optom. Vis. Sci.* **81**, 99–110 (2004).
65. Zhou, X. et al. Biometric measurement of the mouse eye using optical coherence tomography with focal plane advancement. *Vis. Res.* **48**, 1137–1143 (2008).
66. Bais, A. S. & Kostka, D. scds: computational annotation of doublets in single-cell RNA sequencing data. *Bioinformatics* **36**, 1150–1158 (2020).
67. Hao, Y. et al. Integrated analysis of multimodal single-cell data. *Cell* **184**, 3573–3587 e3529 (2021).
68. Hafemeister, C. & Satija, R. Normalization and variance stabilization of single-cell RNA-seq data using regularized negative binomial regression. *Genome Biol.* **20**, 296 (2019).
69. Aran, D. et al. Reference-based analysis of lung single-cell sequencing reveals a transitional profibrotic macrophage. *Nat. Immunol.* **20**, 163–172 (2019).
70. Jin, S. et al. Inference and analysis of cell-cell communication using CellChat. *Nat. Commun.* **12**, 1088 (2021).
71. Morabito, S., Reese, F., Rahimzadeh, N., Miyoshi, E. & Swarup, V. hdWGCNA identifies co-expression networks in high-dimensional transcriptomics data. *Cell Rep. Methods* **3**, 100498 (2023).
72. Szeto, J. et al. Regional differences and physiologic behaviors in peripapillary scleral fibroblasts. *Investig. Ophthalmol. Vis. Sci.* **62**, 27 (2021).
73. Zhou, X. et al. Genetic deletion of the adenosine A2A receptor confers postnatal development of relative myopia in mice. *Investig. Ophthalmol. Vis. Sci.* **51**, 4362–4370 (2010).
74. Zhao, F. et al. Dysfunction of VIPR2 leads to myopia in humans and mice. *J. Med. Genet.* **59**, 88–100 (2022).
75. Lu, F. et al. Feasibility of two-dimensional gel electrophoresis used for proteomic analysis of human scleral fibroblasts. *Curr. Eye Res.* **32**, 319–329 (2007).

Acknowledgements

The authors thank Peter S. Reinach (Wenzhou Medical University, China), William K. Stell (University of Calgary, Canada) for their excellent guidance and editing of the manuscript. This study was supported by the National Natural Science Foundation of China 82171096, 81570881 (F.X.Z.), 82025009, 82388101, U23A20438 (X.T.Z.), 82422019, 82171097 (F.Z.), U20A20364 (J.Q.), 32571524 (W.C.); Zhejiang Provincial Natural Science Foundation of China LY22H120001 (F.X.Z.); and the Innovative research team of high-level local universities in Shanghai (X.T.Z.).

Author contributions

X.T.Z., F.X.Z., F.Z., and J.Q. designed and supervised the study; H.Z., F.X.Z., X.M.L., S.M.J., L.Y., H.H.L., M.Y.D., Y.X.Z., Y.L.P., and Z.L.Z.,

performed animal and cell experiments, reverse transcription quantitative polymerase chain reaction, RNA FISH, immunofluorescence, western blotting, transmission electron microscopy, and the data analysis; W.C. and F.Z., performed bioinformatics analysis of single-cell RNA sequencing and bulk RNA sequencing; F.X.Z. and W.C. wrote original draft; F.X.Z., W.C., H.Z., J.Q., F.Z., and X.T.Z., reviewed and revised the manuscript; F.X.Z., J.Q., F.Z., and X.T.Z., acquired funding. All authors have read and approved the current version of this manuscript and have agreed to its submission.

Competing interests
The authors declare no competing interests.

Additional information
Supplementary information The online version contains supplementary material available at https://doi.org/10.1038/s41467-025-67246-x.

Correspondence and requests for materials should be addressed to Fei Zhao, Fuxin Zhao or Xiangtian Zhou.

Peer review information *Nature Communications* thanks Baptiste Wilmet, and the other, anonymous, reviewer(s) for their contribution to the peer review of this work. A peer review file is available.